DEGREE PROJECT IN MECHANICAL ENGINEERING,
SECOND CYCLE, 30 CREDITS
STOCKHOLM, SWEDEN 2017

Numerical Model of Melting Problems

A Model Based on an Enthalpy-Porosity Approach for the Study of Phase Change Problems inside a 2D Cavity

ARTURO AROSEMENA

KTH ROYAL INSTITUTE OF TECHNOLOGY
SCHOOL OF ENGINEERING SCIENCES

Numerical Model of Melting Problems

A Model Based on an Enthalpy-Porosity Approach for the Study of Phase Change Problems inside a 2D Cavity

ARTURO AROSEMENA

Master of Science Thesis
Supervisor and Examiner: Professor Luca Brandt, PhD
KTH Royal Institute of Technology
School of Engineering Sciences
Department of Mechanics
SE-100 44 Stockholm, Sweden

Abstract

In the present study, a finite volume method is employed to model the advection-diffusion phenomenon during a pure substance melting process. The exercise is limited to a benchmark problem consisting of the 2D melting from a vertical wall of a PCM driven by natural convection in the melt. Numerical results, mainly the temporal evolution of average Nusselt number at the hot wall and the average liquid fraction, are validated by available literature data and the effect of thermal inertia in the heat transfer is considered as well. Finally, motivated by recent publications and the model presented here, possible new research topics are proposed.

Keywords: Phase change materials, fluid dynamics, heat transfer, natural convection, melting, enthalpy-porosity technique.

Acknowledgements

I would like to express my appreciation to the KTH Mechanics and KTH Centre of Naval Architecture personnel involved in my education during the programme. It has been a remarkable academic enrichment experience.

My sincere gratitude to Professor Luca Brandt for supervising and examining my thesis work. I also want to thank Marco Rosti and Francesco de Vita for taking the time to read the thesis and for the provided feedback.

Last but not least, I would like to convey my thanks to my mother and grandmother who continuously support me and to my dear Angelica for her patience, understanding and unconditional affection.

This graduation work has been produced during my scholarship period at KTH Royal Institute of Technology thanks to a Swedish Institute scholarship.

Contents

List of Figures

List of Tables

Chapter 1

Introduction

The melting/solidification of a substance due to natural convection occurs in a wide range of settings and during the last decades a growing interest for the fundamentals behind the heat transfer and fluid dynamics during the melting/solidification process have been motivated particularly by the potential of phase change materials (PCMs) to store energy. The major advantages of latent heat stores under study are their high energy storage density (i.e. large thermal capacity per unit volume) and their almost isothermal behaviour during the phase-change phenomena. Such potential as energy stores makes PCMs an important component in the future smart grid energy strategy (e.g. consider their planned usage in the sustainable residential housing KTH's project, KTH Live-In Lab).

A review on the development of latent heat thermal energy storage materials and systems may be found on Agyenim et al. [1], Zalba et al. [2], Farid et al. [3], and Sharma et al. [4]. Agyenim et al. [1] investigated the criteria that govern the selection of PCMs, the melting temperature range for different practical applications, the geometry and configurations of PCM containers, the heat transfer in PCMs and enhancing techniques, and a series of studies to assess the effects of certain parameters in the heat transfer. Here it is concluded that in terms of problem formulation, the common approach has been the use of an enthalpy formulation for the phase change study involving convection as a heat transfer mechanism in the melt. Zalba et al. [2] did an extensive review with respect to materials employed for thermal energy storage listing more than 150 PCMs, their classification, and some applications. Farid et al. [3] and Sharma et al. [4] studied the classification, properties, and major application of PCMs as well. However

Sharma et al. [4] also considered the heat transfer characteristics of the melting/solidification process and different techniques for solving phase change problems. Here the advantages of using the enthalpy formulation are remarked (e.g. governing equation is similar to the single phase equation, condition on solid-liquid interface is automatically satisfied, and it allows a mushy zone region between the two phases).

Concrete examples of applications such as cooling of electronics, solar collectors, and thermal control in the construction of lightweight structures may be found on Kandasamy, Wang, and Mujumdar [5], Mettawee and Assassa [6], and Kuznik, Virgone, and Noel [7].

Most of the available experimental and numerical results have been obtained for the melting of pure phase change materials. In the context of numerical studies, a large number of papers dedicated to this topic may be found in literature. However Bertrand et al. [8] and Gobin and Le Quéré [9] may be considered a benchmark in the sense that a systematically comparison of independent algorithms to solve a relatively simpler problem, the melting of a pure substance driven by natural convection in the melt, is made.

The study of the advection-diffusion phenomenon and its modelling during a pure substance melting process inside a 2D cavity is the main purpose of this thesis. The exercise is limited to the aforementioned benchmark problem consisting in the melting from a vertical wall. The main goal is to have a working algorithm which could be modified, possibly with relatively ease, to do new research in the field.

1.1 Thesis Outline

The thesis has been structured in the following way:
-In chapter 1, the study of phase change problems is motivated and it is stated that the research is limited to the 2D melting from a vertical wall of a PCM driven by natural convection in the melt. Also, a brief summary on part of the literature reviewed with respect to PCMs and the model of phase change problems is presented.
-In chapter 2, the mathematical/physical background is indicated.
The general notation to be used is introduced and described: Cartesian coordinates, Cartesian tensors, indicial notation, and common operators/operations appearing in the governing equations.
Also a theory review on transport phenomena is given. Here trans-

port phenomena is understood as the study of momentum, energy, and mass transport, kinematics notions are given as basis for dynamical studies, and the integral and differential form of the conservation equations that govern fluid-flow problems are deduced from basic principles.
-In chapter 3, a brief review on PCMs and the melting of a pure substance is shown. Then a mathematical model for the study of phase change problems based on an enthalpy-porosity approach is proposed.
-In chapter 4, the geometry, boundary conditions, and initial conditions of the problem under consideration are described. Also the test cases corresponding to the different computational runs are exposed.
-In chapter 5, the numerical modelling of the melting problem under consideration is outlined considering aspects such as the spatial discretization, the numerical treatment of the boundary conditions, the iterative process to obtain the liquid fraction and temperature field, and the temporal discretization.
-In chapter 6, the obtained results are qualitatively compared with those of Bertrand et al. [8] and Gobin and Le Quéré [9] and Huber et al. [10] and then quantitatively through the scaling laws and correlations presented in Gobin and Bénard [11] and Jany and Bejan [12] and Huber et al. [10], for the low/high Stefan number range, respectively.
-In chapter 7, the work is concluded with some observations and possible new research topics are proposed.

Chapter 2

Mathematical Background

2.1 General Notation

2.1.1 Cartesian Coordinate System

In general a Cartesian coordinate system is a three dimensional rectilinear coordinate system, i.e. basis vectors are chosen so that the axes are all Euclidean straight lines, which are orthogonal to each other. See figure 2.1.

2.1.2 Cartesian Tensors

An n-th rank Cartesian tensor is a mathematical object that has n indices and 3^n components obeying certain transformation rules. Tensor are used to represent properties of a physical system.

A zero-order tensor represents a scalar. Scalars are completely defined by their magnitude which may vary in space with independence of the coordinate directions (e.g. density and pressure field). In the following chapters scalars are to be denoted using italicized symbols.

A first-order tensor represents a vector. Vectors are completely defined by their magnitude and direction (e.g. velocity field). Hence, in contrast with scalars, vectors do dependent on the coordinate directions. In the following chapters vectors are denoted using boldface symbols. As an example consider the position vector $\mathbf{x}$ seen in figure 2.1 which may be defined as:

$$\mathbf{x} = x_1\mathbf{e_1} + x_2\mathbf{e_2} + x_3\mathbf{e_3}, \qquad \mathbf{e_1} = \begin{bmatrix}1\\0\\0\end{bmatrix}, \quad \mathbf{e_2} = \begin{bmatrix}0\\1\\0\end{bmatrix}, \quad \mathbf{e_3} = \begin{bmatrix}0\\0\\1\end{bmatrix} \tag{2.1}$$

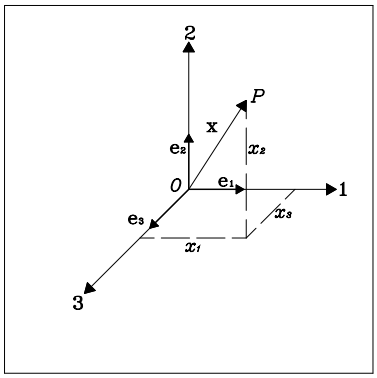

Figure 2.1: Cartesian coordinate system and position vector $\mathbf{x}$. The point O is called the origin of coordinates and the lines $O1$, $O2$, and $O3$ the coordinate axes which are orthogonal to each other. The orthogonality of the coordinate system can also be represented through the use of unit vectors in the direction of the axes, i.e. $\mathbf{e_1}$, $\mathbf{e_2}$, and $\mathbf{e_3}$ in the figure.

Where $\mathbf{x_1}$, $\mathbf{x_2}$, and $\mathbf{x_3}$ are the components of the position vector along each Cartesian axis and $\mathbf{e_1}$, $\mathbf{e_2}$, and $\mathbf{e_3}$ are unit vectors in the direction of the coordinate axis and here are written as column matrixes.

A second-order tensors have 9 separate components and represents physical quantities such as mechanical stress.

2.1.3 Indicial Notation

Indicial notation is a notation introduced to have a more compact and simple representation, particularly when one is dealing with vectors, tensors, and their identities.

Indicial notation is characterized by two important features: the free index and the notational convention.

A free index is an index that appears only once per term and that is not summed over. Vectors and tensor may be represented with the use of free indexes. Consider for example the position vector $\mathbf{x}$ which using indicial notation may be written as $\mathbf{x} = (x_1, x_2, x_3) = e_i x_i$ or simply x_i where the index i is the free index and can take the value 1, 2, or 3. A second-order tensor is represented by two free indexes, e.g.

σ_{im} representing the tensor:

$$\sigma_{im} = \begin{bmatrix} \sigma_{11} & \sigma_{12} & \sigma_{13} \\ \sigma_{21} & \sigma_{22} & \sigma_{23} \\ \sigma_{31} & \sigma_{32} & \sigma_{33} \end{bmatrix} \tag{2.2}$$

The notational convention (also called Einstein summation convection) is an implicit convention stating that repeated indexes are summed over, i.e. $a_i a_i \equiv \sum_{i=1}^{3} a_i a_i$. In this case the index i is a summation or "dummy" index which may be replaced by another symbol (e.g. j or m) without changing the meaning of the expression.

2.1.4 Kronecker Delta and Permutation Symbol

The Kronecker delta δ_{im} is an isotropic (components change by a rotation of the frame of reference) second-order tensor which in a three dimensional space is the identity matrix, i.e.

$$\delta_{im} = \begin{bmatrix} 1 & 0 & 0 \\ 0 & 1 & 0 \\ 0 & 0 & 1 \end{bmatrix} \tag{2.3}$$

In matrix multiplication involving the Kronecker delta, it is important to emphasis the following identity $\delta_{im} x_m = x_i$.

The alternating tensor or permutation symbol ϵ_{ijk} is an isotropic third-order tensor (i.e. with 3^3 components) defined as:

$$\epsilon_{ijk} = \begin{cases} 1, & \text{if } ijk \text{ present cyclic order (e.g. } ijk = 312) \\ 0, & \text{if any two indices are equal (e.g. } ijk = 322) \\ -1, & \text{if } ijk \text{ present anti-cyclic order (e.g. } ijk = 132) \end{cases} \tag{2.4}$$

By definition the following identities apply to the alternating tensor, $\epsilon_{ijk} = \epsilon_{jki}$, $\epsilon_{ijk} = -\epsilon_{jik}$. Another important identity is the epsilon-delta relation $\epsilon_{ijk}\epsilon_{klm} = \delta_{il}\delta_{jm} - \delta_{im}\delta_{jl}$.

2.1.5 Common Operators and Operations

In the following lines some common operators and operations are introduced.

The Nabla operator $\boldsymbol{\nabla}$ is defined as:

$$\boldsymbol{\nabla} = \left(\frac{\partial}{\partial x_1}, \frac{\partial}{\partial x_2}, \frac{\partial}{\partial x_3} \right) = e_i \frac{\partial}{\partial x_i} \tag{2.5}$$

The Laplace operator $\boldsymbol{\nabla^2}$ is defined as:

$$\boldsymbol{\nabla^2} = \left(\frac{\partial^2}{\partial {x_1}^2} + \frac{\partial^2}{\partial {x_2}^2} + \frac{\partial^2}{\partial {x_3}^2} \right) = \frac{\partial^2}{\partial {x_i}^2} \tag{2.6}$$

The dot product $(\cdot)$ of two vectors $\mathbf{a}$ and $\mathbf{b}$ is defined as:

$$\mathbf{a} \cdot \mathbf{b} = \mathbf{b} \cdot \mathbf{a} = a_i b_i \tag{2.7}$$

The cross product $(\times)$ of two vectors $\mathbf{a}$ and $\mathbf{b}$ is defined as:

$$\mathbf{a} \times \mathbf{b} = \det \begin{bmatrix} \mathbf{e_1} & \mathbf{e_2} & \mathbf{e_3} \\ a_1 & a_2 & a_3 \\ b_1 & b_2 & b_3 \end{bmatrix} = \epsilon_{ijk} a_i b_j \tag{2.8}$$

The gradient of a scalar is the application of the Nabla operator over a scalar field f leading to a vector field:

$$\boldsymbol{\nabla} f = e_i \frac{\partial f}{\partial x_i} \tag{2.9}$$

The divergence of a vector is the dot product between the Nabla operator and a vector field $\mathbf{a}$ leading to a scalar field:

$$\boldsymbol{\nabla} \cdot \mathbf{a} = \frac{\partial a_i}{\partial x_i} \tag{2.10}$$

In case of a second-order tensor $\boldsymbol{\sigma} = \sigma_{im}$, its divergence leads to a vector field with i-component defined as:

$$(\boldsymbol{\nabla} \cdot \boldsymbol{\sigma})_{\mathbf{i}} = \frac{\partial \sigma_{im}}{\partial x_m} \tag{2.11}$$

The curl of a vector is the cross product between the Nabla operator and a vector field $\mathbf{a}$, with i-component defined as:

$$(\boldsymbol{\nabla} \times \mathbf{a})_{\mathbf{i}} = \epsilon_{ijk} \frac{\partial a_k}{\partial x_j} \tag{2.12}$$

It must be noted that a vector $\mathbf{a}$ is called divergence free if $\boldsymbol{\nabla} \cdot \mathbf{a} = 0$ and irrotational if $(\boldsymbol{\nabla} \times \mathbf{a})_{\mathbf{i}} = 0$.

2.2 Transport Phenomena

2.2.1 Overview about Transport Phenomena

Transport phenomena concern the study of momentum, energy, and mass transport. Historically, these transport phenomena were treated independently and covered through Fluid Dynamics and Heat and Mass Transfer studies. However, during the last century or so, interdisciplinary applications (e.g. meteorology, biotechnology, and micro/nanotechnology) and the inherent analogies between all types of transports have led to their unified study.

There are three levels at which transport phenomena can be studied: macroscopic, microscopic and molecular. At the macroscopic level, the entities (i.e. mass, momentum, and energy) change due to their introduction and removal via entering and leaving streams and because of the system interaction with the surroundings. Here "macroscopic balances" are formulated and there is no interest in understanding what it is happening inside the system. At the microscopic level, one analyse what it is happening to the system in a small region and within such region "equations of change" of all the entities are formulated. The purpose is to acquire information about properties such as velocity, temperature, and pressure within the system. Meanwhile, at the molecular level, one seek to understand the transport phenomena in terms of the molecular structure and intermolecular forces. It must be noted that there are different "length scales" associated with each level, e.g. centimetres or meters at macroscopic level compared to nanometres at molecular level [13].

At this point, it is important to point out that all the transport phenomena involve both molecular transport denoted as diffusion (i.e. transport from high concentration to low concentration of the corresponding entity) and bulk flow motion transport denoted as advection (i.e. transport of the corresponding entity by the fluid flow).

The term advection is used instead of convection to avoid misunderstanding with the heat transfer mechanism.

2.2.2 Fluid Kinematics

Kinematics is the study of motion without considering the forces that produce it.
Hence the results from kinematics studies apply to all type of fluid and

are the base on which dynamical results are constructed [14].

Before introducing some notions about fluid kinematics, it is important to discuss the continuum hypothesis: for a large enough region, the actual discrete properties (e.g. pressure, temperature, and density at molecular level) are treated as spatial point properties varying continuously in space and time. Such properties consist on the averages of molecular characteristics in a small region surrounding the point of interest. The continuum approximation is valid when the Knudsen number, representing the ratio of the mean free path of the molecules and the length scale of interest, is much less than unity [15].

Descriptions of Fluid Motion

The motion in a fluid treated as a continuum is described using either material coordinates (also called Lagrange coordinates) or spatial coordinates (also called Euler coordinates). In a material description each fluid particle (i.e. point of interest where properties consist on the averages of the molecular characteristics) is marked and followed through the flow field while in a spatial description a fixed point in space is considered and the flow field is observed from this point. Hence in the first case, the flow kinematic is described by the initial position of the fluid particle and time while in the second case, it is described both by space coordinates, e.g. Cartesian coordinates: x_1, x_2, x_3 and time.

An understanding of both description is required. For example, the acceleration following a fluid particle is needed for the application of Newton's second law to fluid motion while observations of fluids flows are usually made at fixed locations with the fluid moving past that location [15].

Material Time Derivative

The material time derivative is the rate of change in time as observed when moving with the fluid particle expressed in spatial coordinates.

Consider that a certain fluid particle is at an initial position ${x_i}^0 = ({x_1}^0, {x_2}^0, {x_3}^0)$ and at a later time t the same particle is at a position $x_i = (x_1, x_2, x_3)$. Thus the particle path is described as $x_i = x_i\,({x_i}^0, t)$. Where the initial coordinate ${x_i}^0$ is the material coordinate whilst x_i is the spatial coordinate of the fluid particle.

Here, it is also assumed that the motion is continuous, single value and that one can invert the expression describing the particle path to

give the initial position of the particle at any position x_i at a time t. Hence ${x_i}^0 = {x_i}^0(x_i, t)$, it is also continuous and single value. Assumptions must also extent to the derivatives. A necessary and sufficient condition for the inverse functions to exist is that the Jacobian determinant J should not be equal to zero, i.e. $J = |\partial x_i / \partial {x_i}^0| \neq 0$.

Now, consider a quantity U following the particle, where $U = U_L({x_i}^0, t) = U_E(x_i({x_i}^0, t), t)$. The sub-index L and E denote Lagrange and Euler description, respectively.

The material or substantial time derivative D/Dt is then given by:

$$\frac{DU}{Dt} = \left.\frac{\partial U_L}{\partial t}\right|_{{x_i}^0} = \left(\frac{\partial U_E}{\partial t}\right)\left(\frac{\partial t}{\partial t}\right) + \left(\frac{\partial U_E}{\partial x_i}\right)\left(\frac{\partial x_i}{\partial t}\right) \tag{2.13}$$

$$\frac{DU}{Dt} = \frac{\partial U_E}{\partial t} + u_i \frac{\partial U_E}{\partial x_i} \tag{2.14}$$

Consequently the material time derivative allows to express the rate of change for the material fluid element property in terms of the rate of change at a fixed position in space and the advection rate of change as the fluid particle moves through the spatial gradients of the property.

In the expression above the summation convention is used (see section 2.1.3., e.g. $u_k u_k \equiv u_1 u_1 + u_2 u_2 + u_3 u_3$) and the velocity field components are defined as $u_i = (u_1, u_2, u_3)$.

Consider as an example U equal to the velocity field:

$$\frac{Du_j}{Dt} = \frac{\partial u_j}{\partial t} + u_i \frac{\partial u_j}{\partial x_i} \tag{2.15}$$

Therefore the substantial time derivative of the velocity field represents the acceleration of the material fluid element.

Deformation of Material Fluid Elements

In a fluid as a material that deforms continuously under the action of shear stress, a basic constitutive law for the fluid (e.g. Newton phenomenological relationship) relates fluid element deformation rate to stresses applied to the fluid element [15].

The deformation of a material fluid element is due to the relative motion between two nearby particles. Such relative motion can be describe knowing the velocity gradient second order tensor, i.e. $\partial u_i / \partial x_j$.

The velocity gradient tensor can be decomposed in the following tensors:

$$\frac{\partial u_i}{\partial x_j} = S_{ij} + R_{ij}, \qquad S_{ij} = \overline{S}_{ij} + \overline{S}_{mm} \tag{2.16}$$

Where S_{ij} is the symmetric part (i.e. $S_{ij} = S_{ji}$) known as the strain rate tensor (i.e. rate of deformation) and R_{ij} is the antisymmetric part (i.e. $R_{ij} = -R_{ji}$) known as the rotation tensor. $\overline{S}_{ij}$ and $\overline{S}_{mm}$ represent the traceless and isotropic part of S_{ij}, respectively.

The respective tensors are denoted by:

$$S_{ij} = \frac{1}{2}\left(\frac{\partial u_i}{\partial x_j} + \frac{\partial u_j}{\partial x_i}\right), \qquad R_{ij} = \frac{1}{2}\left(\frac{\partial u_i}{\partial x_j} - \frac{\partial u_j}{\partial x_i}\right) = -\epsilon_{ijk}\frac{\omega_k}{2} \tag{2.17}$$

$$\overline{S}_{ij} = \frac{1}{2}\left(\frac{\partial u_i}{\partial x_j} + \frac{\partial u_j}{\partial x_i} - \frac{2}{3}\frac{\partial u_m}{\partial x_m}\delta_{ij}\right), \qquad \overline{S}_{mm} = \frac{1}{3}\frac{\partial u_m}{\partial x_m}\delta_{ij} \tag{2.18}$$

Here ω_k is the vorticity vector (i.e. rotational of the flow velocity vector).

In summary, the motion of a fluid particle with velocity u_i can be divided into the following invariant parts: solid body translation due to u_i, solid body rotation due to R_{ij}, deviation change in shape (i.e. volume constant deformation) due to $\overline{S}_{ij}$, and isotropic compression/expansion due to $\overline{S}_{mm}$ [16].

Reynolds Transport Theorem

The Reynolds Transport Theorem is an important kinematical theorem due to Reynolds and concerns the rate of change of any volume integral [14].

Consider the time derivative of an arbitrary entity volume integral, where the volume is moving with the fluid (i.e. material volume) as depicted in figure 2.2:

$$\begin{aligned}\frac{D}{Dt}\int\limits_{V(t)} U_{ij}dV = &\lim_{\Delta t\to 0}\left\{\frac{1}{\Delta t}\int\limits_{V(t+\Delta t)} U_{ij}\left(t+\Delta t\right)dV\right\} \\ &- \lim_{\Delta t\to 0}\left\{\frac{1}{\Delta t}\int\limits_{V(t)} U_{ij}\left(t\right)dV\right\}\end{aligned} \tag{2.19}$$

$$\begin{aligned}\frac{D}{Dt}\int\limits_{V(t)} U_{ij}dV = &\lim_{\Delta t\to 0}\left\{\frac{1}{\Delta t}\int\limits_{V(t+\Delta t)} U_{ij}\left(t+\Delta t\right)dV\right\}\\ &-\lim_{\Delta t\to 0}\left\{\frac{1}{\Delta t}\int\limits_{V(t)} U_{ij}\left(t+\Delta t\right)dV\right\}\\ &+\lim_{\Delta t\to 0}\left\{\frac{1}{\Delta t}\int\limits_{V(t)} U_{ij}\left(t+\Delta t\right)dV\right\}\\ &-\lim_{\Delta t\to 0}\left\{\frac{1}{\Delta t}\int\limits_{V(t)} U_{ij}\left(t\right)dV\right\}\end{aligned} \tag{2.20}$$

Where Δt represents a time interval.

The first difference may be re-written as a closed surface integral, considering that $dV = u_m n_m \Delta t dS$, where n_m is a unit outward vector to the material surface S. The last difference may be recast exactly as the partial derivative respect to time of the arbitrary quantity U_{ij} (e.g. scalar or vector). Hence:

$$\frac{D}{Dt}\int\limits_{V(t)} U_{ij}dV = \oint\limits_{S(t)} U_{ij}u_m n_m dS + \int\limits_{V(t)} \frac{\partial U_{ij}}{\partial t}dV \tag{2.21}$$

The surface integral can be changed back to a volume integral through the divergence theorem:

$$\frac{D}{Dt}\int\limits_{V(t)} U_{ij}dV = \int\limits_{V(t)} \left[\frac{\partial U_{ij}}{\partial t} + \frac{\partial\left(u_m U_{ij}\right)}{\partial x_m}\right]dV \tag{2.22}$$

2.2.3 Conservation Laws

In general a conservation law for a quantity U_{ij} may be stated as: the variation of the total amount of U_{ij} inside a given domain is equal to the balance between the amount of that quantity entering and leaving the considered domain (i.e. net flux of quantity), plus the contributions from eventual sources generating that quantity in the domain. Here,

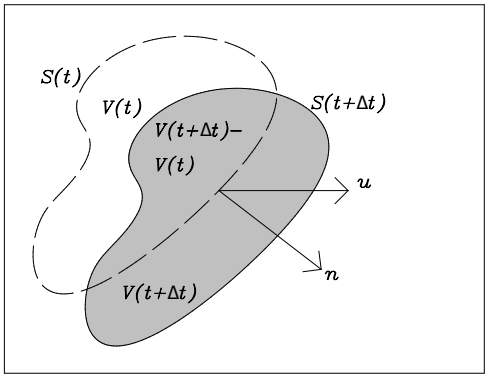

Figure 2.2: Material volume $V(t)$.

one is interested in the rate of change of the quantity U_{ij} [16]. At this point, it must be noted that not all flow quantities are conserved.

With the observation above or through the Reynolds Transport Theorem previously presented, it is possible to derive the conservation laws or transport equations of the following entities: mass, momentum, and energy.

Conservation of Mass

Taking the arbitrary quantity equal to the pure fluid density ρ, from equation (2.22):

$$\frac{D}{Dt}\int\limits_{V(t)} \rho dV = \int\limits_{V(t)} \left[\frac{\partial \rho}{\partial t} + \frac{\partial \left(u_m \rho\right)}{\partial x_m}\right] dV \tag{2.23}$$

The right hand side represent the material time derivative of mass in the material volume, which is conserved, and consequently this term is equal to zero.

Since the expression above must be valid for any arbitrary volume, the differential form of the mass transport equation is:

$$\frac{\partial \rho}{\partial t} + \frac{\partial}{\partial x_m}\left(u_m \rho\right) = 0 \tag{2.24}$$

This equation is known as the continuity equation. The first term of the expression represents the accumulation or rate of increase of mass per unit volume in the fixed element while the second term is the net outward mass flow rate per unit volume of the element due to advection.

It is important to emphasise that in case of mixture, the expression above is the continuity equation of the mixture with constant mass density ρ. Hence there is no diffusion of mass due to differences of species concentrations in the mixture.

Conservation of Momentum

Taking the arbitrary quantity equal to the fluid momentum per unit volume ρu_i, from equation (2.22):

$$\frac{D}{Dt}\int\limits_{V(t)} \rho u_i dV = \int\limits_{V(t)} \left[\frac{\partial(\rho u_i)}{\partial t} + \frac{\partial\left(u_m \rho u_i\right)}{\partial x_m}\right] dV \tag{2.25}$$

Here the right hand side of the expression represents the rate of change of momentum per unit volume in the material element and according to Newton's second law is equal to the sum of all forces, in this case per unit volume, acting on the element. Such forces include both body forces (i.e. acting over the element with physical contact), e.g. gravitational, magnetic, or electrostatic forces, and surface forces (i.e. acting through direct contact with the fluid element), e.g. forces due to pressure and viscous effects.

Therefore:

$$\int\limits_{V(t)} \rho \frac{Du_i}{Dt} dV = \int\limits_{V(t)} F_i dV + \int\limits_{S(t)} W_i dS \tag{2.26}$$

Here F_i represents the body forces per unit volume and W_i represents the surface forces per unit area on surface dS with outward unit normal vector n_m.

One can divide the surface forces into components along the coordinate directions, i.e. $W_i = \tau_{im} n_m$, where τ_{im} is the stress tensor and it is the i-component of the surface force on a surface dS with a normal in the n-direction. Further, it can be shown that the stress tensor is symmetric, i.e. $\tau_{im} = \tau_{mi}$ [15].

The stress tensor can be decomposed into fluid static (due to pressure p) and fluid dynamic (due to viscous stresses σ_{im}) contributions as $\tau_{im} = -p\delta_{im} + \sigma_{im}$.

Now a constitutive equation is required, i.e. an expression to relate viscous stresses to deformation in the continuum. In case of Newtonian fluids, phenological observations have established a linear constitutive equation between stresses and velocity gradients. Thus, for an isotropic fluid:

$$\sigma_{im} = \lambda \overline{S}_{kk} + 2\mu \overline{S}_{im} \tag{2.27}$$

Where λ is the dilatational viscosity and μ is the dynamic viscosity. $\overline{S}_{im}$ and $\overline{S}_{kk}$ are the traceless and isotropic part of the strain rate tensor (see section 2.2.2), respectively.

With the above, equation (2.26) may be recast as:

$$\int\limits_{V(t)} \rho \frac{Du_i}{Dt} dV = \int\limits_{V(t)} F_i dV + \int\limits_{S(t)} \left[-p\delta_{im} + \lambda \overline{S}_{kk} + 2\mu \overline{S}_{im} \right] n_m dS \tag{2.28}$$

Considering the divergence theorem to transform the surface integral into a volume integral and the fact that the above shall hold for an arbitrary volume, one can find the differential form of transport equation corresponding to linear momentum conservation:

$$\begin{aligned} \rho \frac{Du_i}{Dt} &= F_i - \frac{\partial p}{\partial x_i} \\ &+ \frac{\partial}{\partial x_m} \left[\mu \left(\frac{\partial u_i}{\partial x_m} + \frac{\partial u_m}{\partial x_i} - \frac{2}{3} \frac{\partial u_k}{\partial x_k} \delta_{im} \right) + \frac{\lambda}{3} \frac{\partial u_k}{\partial x_k} \delta_{im} \right] \end{aligned} \tag{2.29}$$

Conservation of Energy

Taking the arbitrary quantity equal to the product of the fluid density and the sum of internal energy per unit mass e (i.e. energy associate with the kinetic energy of molecules with respect to the flow velocity and the intermolecular potential energies) and the kinetic energy per unit mass $0.5 u_i u_i$ associate with the bulk fluid motion,
from equation (2.22):

$$\begin{aligned} \frac{D}{Dt} \int\limits_{V(t)} \rho \left(e + \frac{1}{2} u_i u_i \right) dV &= \int\limits_{V(t)} \frac{\partial}{\partial t} \left[\rho \left(e + \frac{1}{2} u_i u_i \right) \right] dV \\ &+ \int\limits_{V(t)} \frac{\partial}{\partial x_m} \left[u_m \rho \left(e + \frac{1}{2} u_i u_i \right) \right] dV \end{aligned} \tag{2.30}$$

The right hand side term represents the rate of change of total energy in the material fluid element which according to the first law of thermodynamics is equal to the rate of energy received by transport of heat plus the execution of work on the fluid (due to body and surface forces).

$$\begin{aligned}\frac{D}{Dt}\int\limits_{V(t)} \rho\left(e+\frac{1}{2}u_i u_i\right)dV &= \int\limits_{V(t)} F_i u_i dV + \int\limits_{S(t)} \left[T_{im}u_m - q_i\right] n_i dS \\ &= \int\limits_{V(t)} \left[F_i u_i + \frac{\partial}{\partial x_i}\left(T_{im}u_m - q_i\right)\right] dV\end{aligned} \tag{2.31}$$

Here q_i is heat flux vector per unit area.

Since the expression above must be valid for any arbitrary volume, the differential form of the energy transport equation is:

$$\rho\frac{D}{Dt}\left(e+\frac{1}{2}u_i u_i\right) = F_i u_i + \frac{\partial}{\partial x_i}\left(T_{im}u_m - q_i\right) \tag{2.32}$$

The total energy transport equation can be split into an equation for the transport of mechanical energy and an equation for the transport of thermal energy. The mechanical energy equation can be found by taking the dot product between the transport equation for momentum and the velocity field. The thermal energy equation is then found subtracting the mechanical energy equation to the total energy transport equation, hence:

$$\rho\frac{De}{Dt} = -p\frac{\partial u_i}{\partial x_i} + \sigma_{im}\frac{\partial u_i}{\partial x_m} - \frac{\partial q_i}{\partial x_i} \tag{2.33}$$

Where the first and second term at the right hand side represent the thermal energy generation due to isotropic compression and the viscous dissipation $\Phi = \sigma_{im}\left(\partial u_i/\partial x_m\right)$, respectively.

The heat flux equally may be rewritten using Fourier phenological relationship:

$$q_i = -k\frac{\partial T}{\partial x_i} \tag{2.34}$$

Where k is the thermal conductivity and it is a function of the thermodynamic state and thus depends on the temperature field T.

The thermal energy equation might be alternatively expresses in terms of the specific enthalpy $h = e + p/\rho$, taking into account the

following:

$$\frac{Dh}{Dt} = \frac{De}{Dt} + \frac{1}{\rho}\frac{Dp}{Dt} - \frac{p}{\rho^2}\frac{D\rho}{Dt} \tag{2.35}$$

Where $D\rho/Dt = -\rho\,(\partial u_i/\partial x_i)$, consequently the thermal energy transport equation may be recast as:

$$\rho\frac{Dh}{Dt} = \frac{Dp}{Dt} + \Phi + \frac{\partial}{\partial x_i}\left(k\frac{\partial T}{\partial x_i}\right) \tag{2.36}$$

It must be noted that radiation as heat transfer mechanism has been neglected.

Chapter 3

Melting and Phase Change Materials

3.1 Phase change materials (PCMs)

In a liquid or solid medium the thermal energy may be stored in the form of sensible heat and in the form of latent heat. A PCM is a latent heat storage material which typically operates over a small temperature range and it is charged during its melting and discharged during its solidification. In other words, energy is transferred to/from the PCM in the form of latent heat during the phase-change process.

In general, PCMs are classified in organic (e.g. paraffin), inorganic (e.g. metals) and eutectic (e.g. organic-organic or organic-inorganic compounds). And depending on the properties/initial conditions of the PCM, a melting (or solidification) problem may be classified as one region, two regions, or three regions (see figure 3.1).

3.2 Melting of a Pure Substance

Heat is thermal energy that it is transferred because of a temperature difference. In the absence of thermal radiation as a heat transfer mechanism, the exchange of heat involves both conduction and convection. Conduction is the thermal energy transferred due to molecular diffusion whilst convection is the transfer of thermal energy due to molecular diffusion and advection associate with bulk fluid motion. Typically, convection is regard as forced if the fluid is forced to flow by external means (e.g. using a pump or fan) and free or natural if the motion is driven by temperature gradients which create density differences in

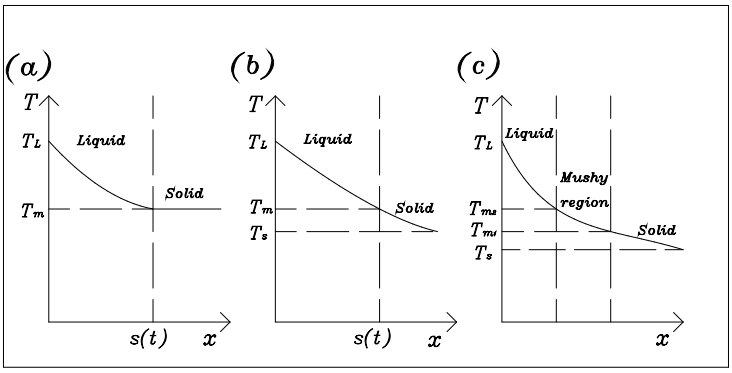

Figure 3.1: Classification of a melting problem in 1D: (*a*) one region, (*b*) two regions, and (*c*) three regions. Here T, x, and s stands for temperature field, spatial coordinate, and the melting front position, respectively. The sub-index l, s, and m stands for liquidus, solidus, and melting point, respectively.

the fluid and induce buoyancy forces (e.g. "cooling" of a boiled egg or a potato in air). In this sense, heat transfer processes involving a phase change are also considered to be convection on account of the fluid motion induced during the process [17].

In general, it is convenient to work with the non-dimensional form of the governing equations (e.g. for easy comparison with other research results, to gain a better understanding of the physical problem, and to reduce the number of independent parameters) using the appropriate scaling parameters. And such procedure introduces certain dimensionless variables in the dimensionless form of the governing equations.

In case of natural convection, there are certain dimensionless parameters associate with this physical mechanism: the Prandtl number Pr which is the ratio of molecular diffusivity of momentum to molecular diffusivity of heat (i.e. ratio of momentum and heat dissipation rate through the fluid), the Grashof number Gr which is the ratio of buoyancy forces (driven by temperature gradients) and viscous forces acting on the fluid, the Rayleigh number Ra which is the product of the Grashof and Prandtl numbers and that actually determines the onset

of natural convection, the Stefan number St which is the ratio between sensible heat and latent heat and that plays an important role in phase change problems, the Fourier number Fo which is the time of thermal diffusion across the reference length, and the Nusselt number Nu which is the ratio between convective and conductive heat transfer.

All previously mentioned dimensionless parameters are introduced in detail during the next sections and chapters but their physical significance is explained at this point with the purpose of discussing the melting of a pure substance.

Jany and Bejan [12] for simple 2D geometries and high Prandtl numbers predicted a four-regime model (view figure 3.2) during the melting process of a pure substance. This four-regime model was employed to propose a group of scaling laws and the corresponding heat correlations.

Initially conduction dominates, see figure 3.2(*a*), and $Nu \propto (StFo)^{-1/2} + Ra(StFo)^{3/2}$, $(StFo) \rightarrow 0$ where the product $StFo$ is the dimensionless time. This is an important conclusion indicating that, relative to the dominant effect (i.e. conduction), the convection contribution increases with time.

As seen from figure 3.2(*b*), the conductive dominant regime is followed by a mixed regime where part of the cavity is affected mainly by convection and part mainly by conduction. The previous expression for the Nusselt number holds during the mixed regime which end when the convective zone extents to the height of the cavity at a corresponding $StFo_1 \propto Ra^{-1/2}$. In the interval $[0, (StFo)_1]$ the Nusselt scaling law characterize itself by the analytical prediction of a minimum Nusselt number $Nu_{min} \propto Ra^{1/4}$ which occurs at a dimensionless time $(StFo)_{min} \propto (StFo)_1$.

At a time greater than $(StFo)_1$ convections dominates, see figure 3.2(*c*). Such regime holds up to a time where the melting front reaches the right wall $(StFo)_2 \propto (L/H)\, Ra^{-1/4}$, here L/H represents the inverse of the cavity aspect ratio being L the width and H the height. The convection regime exists only if $(StFo)_2 > (StFo)_1$, hence if $Ra^{1/4} > H/L$. In this regime the Nusselt number reaches a plateau (i.e. state of little or no change) at $Nu \propto Ra^{1/4}$. For low Prandtl numbers, Jany and Bejan [12] proposed to rescale Ra by the product of the Rayleigh and Prandlt numbers. Based on this observation and assuming the melting front does not reaches the right wall, Gobin and Bénard [11] proposed a correlation for the Nusselt number valid for the convection regime.

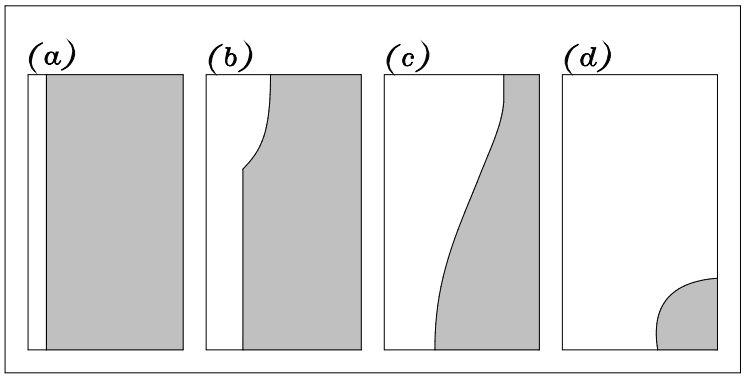

Figure 3.2: Four-regime model predicted by Jany and Bejan [12]: (*a*) conduction regime, (*b*) conduction and convection regime, (*c*) convection regime, (*d*) shrinking solid regime (after the melting front reaches the right wall).

For a time greater than $(StFo)_2$, see figure 3.2(*d*), Jany and Bejan [12] observed that the liquid circulation is always in the convection regime, however the heat transfer and melting rates depend on the size of the remaining solid.

3.3 Governing Equations

The mathematical model for the phase change problem rest on the following assumptions: (1) 2D problem, (2) the flow in the liquid phase is incompressible and Newtonian, (3) surface tension, viscous dissipation and radiation (as a heat transfer mechanism) are neglected, (4) thermophysical properties are constant and uniform, (5) Boussinesq approximation is valid for buoyancy term, and (6) volumetric expansion/contraction due to melting/solidification is neglected.

Consequently equations (2.24), (2.29), and (2.36) with the above assumptions in a Cartesian tensor form are recast as:

$$\frac{\partial u_i}{\partial x_i} = 0 \tag{3.1}$$

$$\rho \frac{Du_i}{Dt} = -\frac{\partial p}{\partial x_i} + \mu \frac{\partial^2 u_i}{\partial x_j \partial x_j} + F_i \tag{3.2}$$

$$\rho \frac{Dh}{Dt} = \frac{Dp}{Dt} + k \frac{\partial^2 T}{\partial x_i \partial x_i} \tag{3.3}$$

Where: (1) the Cartesian coordinates are defined as $x_i = (x_1, x_2) = (x, y)$. Here the positive y axis is pointing upwards and the positive x axis is pointing to the right, (2) the velocity field components are defined as $u_i = (u_1, u_2) = (u, v)$, and (3) the source terms are grouped as $F_i = (F_1, F_2) = (F_x, F_y)$.

Often an enthalpy method is employed for the treatment of phase change problems. In this formulation, the total enthalpy is separated into a sensible heat component and a latent heat component $\Delta h = f_l L$.

Taking into account the above, the energy equation might be recast as:

$$\rho c \frac{DT}{Dt} = \frac{Dp}{Dt} + k \frac{\partial^2 T}{\partial x_i \partial x_i} - \rho \frac{D(f_l L)}{Dt} \tag{3.4}$$

Where c, f_l, and L represent the specific heat, the liquid fraction, and the latent heat, respectively.

For a pure substance, where isothermal phase change takes place, the term $\partial(u_j f_l L)/\partial x_j = 0$ and the liquid fraction is given by the Heaviside step function:

$$f_l = \begin{cases} 0, & T < T_m \\ 1, & T \geq T_m \end{cases} \tag{3.5}$$

However from a computational point of view discontinuities are difficult to track and often it is necessary to smear the phase change over a small temperature range to attain numerical stability [18]. View figure 3.3.

Thus defining $T_s = T_m - \varepsilon$, $T_l = T_m + \varepsilon$ and consequently $h_s = cT_s$, $h_l = cT_l + L$, the liquid fraction may be given by:

$$f_l = \begin{cases} 0, & h < h_s \\ \dfrac{h - h_s}{h_l - h_s}, & h_s \leq h \leq h_l \\ 1, & h > h_l \end{cases} \tag{3.6}$$

The previous expression will hold exact in the case of pure conduction but otherwise it will be a procedure to linearly interpolate the liquid fraction in the phase change region. It must be commented that in this formulation, the liquid fraction is computed at each time step and the phase change interface is not tracked explicitly.

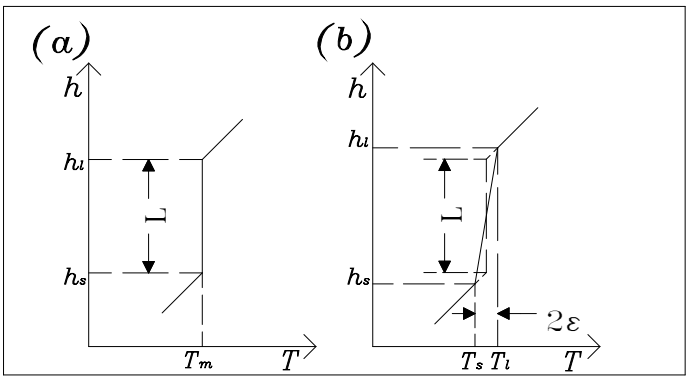

Figure 3.3: Schematic of the enthalpy-temperature relationship: (*a*) pure substance, (*b*) non-pure substance and pure substance with numerical treatment of the discontinuity. Here ε is a phase change interval and for a pure substance is a numerical artificial constant.

The condition that all velocities in solid regions are zero is accounted for through the use of the liquid fraction and a parameter defined so that the momentum equations are forced to mimic the Carman-Koseny relation for a porous medium [19, 20].

The above is known as the enthalpy-porosity approach. The foretold condition is introduced via source terms in the momentum equations as it will be seen next.

The governing equations can be expressed in non-dimensional form with the definition of the appropriate scales. Considering a length, velocity, time, and a temperature difference scales equal to H, $(\mu/\rho_0)/H$, H^2/α, and $T_1 - T_0$, equations (3.1), (3.2), and (3.4) may be recast as:

$$\frac{\partial u_i{}^*}{\partial x_i{}^*} = 0 \tag{3.7}$$

$$\frac{Du_i{}^*}{Dt^*} = -\frac{\partial \tilde{p}^*}{\partial x_i{}^*} + Pr\frac{\partial^2 u_i{}^*}{\partial x_j{}^* \partial x_j{}^*} + S_i{}^* + RaPrT^*\delta_{i2} \tag{3.8}$$

$$\frac{DT^*}{Dt^*} = \frac{\partial^2 T^*}{\partial x_i{}^* \partial x_i{}^*} - \frac{1}{St}\frac{\partial f_l}{\partial t^*} \tag{3.9}$$

Where $Pr = \frac{\mu}{\alpha\rho_0}$, $Ra = \frac{g\rho_0\beta(T_1 - T_0)H^3}{\mu\alpha}$, and $St = \frac{c(T_1 - T_0)}{L}$, respectively. Here: H is the reference length, $\rho = \rho_0$ except for the buoyant term where $\rho = \rho_0[1 - \beta(T - T_0)]$ due to the Boussinesq approximation, $\alpha = k/(c\rho_0)$ is the thermal diffusivity of the fluid, T_0 is a reference temperature and typically the phase change temperature, T_1 is a superheat/supercooling temperature if melting/solidification is being studied, the $*$ super-index signifies a non-dimensional variable, g is the gravity constant acceleration, and β is the coefficient of thermal expansion. Also the change from p to $\tilde{p}$ represents the pressure shift (i.e. $\boldsymbol{\nabla}\tilde{p} = \boldsymbol{\nabla}p + \rho_0 g\delta_{i2}$).

In the momentum equation the source term $F_i{}^*$ is been split into the buoyant term $RaPrT^*\delta_{i2}$ and a Darcy type term $S_i{}^*$ to force the zero velocity condition in the solid region. Also it must be noted the absence of the material time derivative of the non-dimensional pressure in the energy equation due to the incompressible flow hypothesis (the Mach number is assumed to tend to zero).

With regards to the Darcy type source term, the idea is to gradually reduce the velocities from a finite value in the liquid region to zero in the solid. For this purpose the artificial mushy region of the PCM is treated as a "pseudo" porous medium with porosity equal to the liquid fraction [19] as follows:

$$S_i{}^* = A\frac{(1 - f_l)^2}{f_l^3 + \varepsilon}u_i{}^* \tag{3.10}$$

Where the phase change interval ε is introduced simply to avoid zero division and A is a constant that should be adjusted such as the source term is at least seven orders of magnitude higher than all the other terms in the momentum equations in the solid region [18]. It must be commented that A may significantly influence the morphology of the phase front, and care must be taken in its selection [20].

Chapter 4

Proposed Test Cases

4.1 Problem Definition

The simulations are performed for a square cavity initially filled with a PCM as depicted in figure 4.1. This melting problem is driven by natural convection in the melt and the mathematical model described in section 3.3 is employed to obtain the time evolution of the average melting front location and the average Nusselt number at the hot wall.

4.2 Test Cases

The problem is characterized by the Prandtl, Rayleigh, and Stefan numbers, as it can be seen from equations (3.7), (3.8), and (3.9). It does also depend on the cavity global aspect ratio. Similar to Huber et al. [10] two groups of numerical test are considered, corresponding to distinct ranges of the Stefan number: the low range (e.g. $St = 10^{-2}$) and the high range (e.g. $St = 10^{1}$). In the low range, a $Pr = 0.02$ is being used and the results are compared with those of benchmarks Bertrand et al. [8] and Gobin and Le Quéré [9]. In the high range, a $Pr = 1$ is employed and the results are compared with those of Huber et al. [10]. Table 4.1 summarized all numerical runs.

Table 4.1: Test cases corresponding to the two Stefan number ranges.

$St = 0.01$	$Ra = 2.5 \times 10^4$	$Ra = 2.5 \times 10^5$		
$Pr = 0.02$	Case 1	Case 2		
$St = 10$	$Ra = 5 \times 10^4$	$Ra = 1.7 \times 10^5$	$Ra = 8.4 \times 10^5$	$Ra = 6.8 \times 10^6$
$Pr = 1$	Case 3	Case 4	Case 5	Case 6

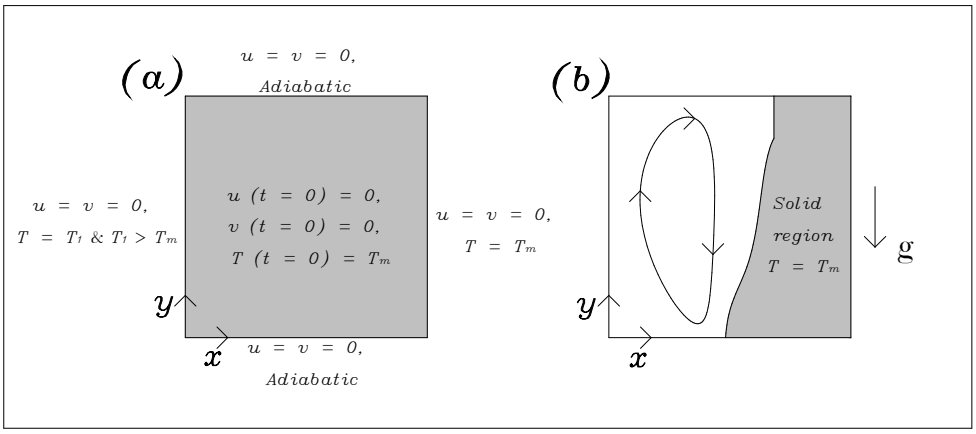

Figure 4.1: Schematic representation of the problem under consideration.

Chapter 5

Numerical Modelling of Melting Problem

5.1 Numerical Methods and Computational Fluid Dynamics

Analytic solutions to transport phenomena problems in literature are rare and mostly involve simplify models, relatively simple geometries and boundary conditions. However, most practical problems entail complex effects, geometries, and boundary conditions and cannot be solve analytically. In such cases, sufficiently accurate approximate solutions can be obtained by computers using a numerical method [17].

An analytical solution imply solving the governing equations in integral or differential form together with the boundary conditions to obtain a continuous solution of the flow variables (e.g. temperature, pressure, and velocity field). In contrast, numerical methods are based on replacing the governing equations in integral or differential form by a set of algebraic, linear or non-linear, equations for the unknown flow variables in selected points inside the media (i.e. discrete points) and simultaneously solving such equations [17]. In this sense, Computational Fluid Dynamics (CFD), is a science that, with the help of digital computers produces quantitatively prediction of fluid-flow phenomena based on the conservation laws governing the fluid motion [15].

There are different types of numerical methods that have been developed to perform transport phenomena simulations in fluid flows. Finite difference method, finite volume method, and finite element method can be listed between the most popular in such CFD compu-

tations.

5.1.1 Discretization Phase in CFD

Once a mathematical model has been used to describe the actual problem based on all relevant physical laws, principles, and assumptions, one can begin the discretization phase in the computational approach. Such phase involves two components: space discretization and equation discretization.

The space discretization consists in setting up a mesh or grid by which the continuum space is replaced by a finite number of points where the numerical value of the variables will have to be determined. Here one can distinguish between structured and unstructured grids. The former is composed of families of intersecting lines, one for each space dimension, being each mesh point located at the intersection of one line, and one line only, of each family (e.g. uniform and non-uniform Cartesian grids). The later, instead, refer to an arbitrary distribution of mesh points where the points are connected by triangles, quadrilaterals, or polygons in 2D and various polyhedral in 3D [21]. It must be emphasis that the accuracy of the obtained numerical results is highly dependent on the mesh quality and typically structured grids are more efficient from a CFD point of view, e.g. more accurate results and less CPU time [21].

The equation discretization refers to the mathematical transformation of the governing equations into an algebraic, linear or nonlinear, system of equations for the discrete flow variables according to the defined mesh. Here an important distinction, regarding time dependent flows, must be made. One can have explicit and implicit methods. In an explicit formulation, the matrix of unknown variables at the new time level is diagonal and it is determine based on previously known values in a trivial manner while in an implicit formulation, the matrix to be inverted is not diagonal since more than one set of variables are unknown at the same time level [21].

5.1.2 Validity and Accuracy of a Numerical Scheme

The obtained set of discretised equations define a determined numerical scheme or method. A quantitative assessment of the validity and accuracy of the numerical scheme is required to validate the obtained

results. Consistency, stability, and convergence form the basis for such quantitative assessment [21].

Consistency is a condition on the numerical scheme; that is the discretized equation must tend to the differential or integral equation as the spatial grid spacing and time step tend to zero. Hence, consistency is related to how well the numerical scheme approximates the mathematical model of the problem, i.e. the truncation error (order of accuracy) of the scheme.

Stability is a condition on the numerical solution; that is all errors of any source (e.g. round off and truncation errors) remain bounded (i.e. do not grow) as the computation proceeds. The stability of a numerical scheme (e.g. absolute stable, conditional stable) can be evaluated through a Von Neumann stability analysis. It must be comment that fully explicit methods are conditionally stable while fully implicit methods are absolute stable.

Convergence is a condition on the numerical solution; that is the numerical solution approaches the exact solution as the spatial grid spacing and time step approach zero. Differently to consistency and stability, it is very difficult to show convergence without knowing the exact solution. However, according to the Lax-Richtmyer equivalence theorem: for a linear, well-posed initial value problem (in the sense of Hadamard) and a consistent discretization scheme, stability is the necessary and sufficient condition for convergence.

5.1.3 The Finite Volume Method

The finite volume method (FVM) is a numerical method in which the continuum is divided into a finite number of small volume elements and where the space discretization is done directly on the integral formulation of the conservation laws. The FVM has the advantage that conservative discretization (i.e. the flux of a quantity entering a finite volume is equal to that leaving the adjacent volume) is satisfied with the integral formulation.

Due to the above, the finite volume method is quite general and can be used either in a structured mesh or in an unstructured one and the unknown variables can be defined either at the centre or at the corner of the grid cells. The first approach is known as cell-centred while the second as cell-vertex.

The FVM in general involves the following step [22]: (1) the do-

main is decomposed into small finite volume elements also known as control volumes, (2) the integral form of the conservation equations is formulate for each control volume, (3) integrals are approximated by numerical integration (e.g. midpoint, trapezoidal, or Simpson rule), (4) function values and derivatives are approximated by interpolation with nodal values (e.g. central differencing and upwind approximations), (5) the resulting set of discrete algebraic equations are rearranged and solved.

An interesting fact is that over a Cartesian, uniform grid the finite volume formulation leads to finite difference formulas which are second order accurate in space (e.g. in 2D, the central finite difference formula appears in the continuity equation and the five point Laplace formula appears in the momentum and energy equations).

5.1.4 Implicit-Explicit Methods for Time Integration of Spatially Discretized Problems

Implicit-Explicit (IMEX) schemes are methods employed to do the temporal integration of spatially discretized time dependent problems. In such methods, some of the time dependent terms show an explicit formulation whilst others an implicit formulation. Typically in diffusion-advection type of problems, an implicit formulation is used for the diffusive term and an explicit one is used for the advective term [23].

There are several popular IMEX schemes that have been used in literature, e.g. first-order forward/backward Euler scheme and second-order Crank-Nicolson/Adams-Bashforth scheme.

It is important to emphasise that since an IMEX scheme is not fully implicit at best it will be conditionally stable.

Second-Order IMEX Schemes

Consider for example a time-dependent partial differential equation in which the spatial derivatives have been discretized using central finite differences or another method. This results in a discrete system of ordinary differential equation in time of the form $d(\mathbf{O})/dt = f(\mathbf{O}) + dg(\mathbf{O})$. Here $\mathbf{O}$ represents the set of unknowns, $f(\mathbf{O})$ is some possible nonlinear term which it is to be integrated explicitly, d is a non-negative parameter, and $gf(\mathbf{O})$ is the term that it is to be integrated implicitly to avoid excessively small time steps [23].

A second-order IMEX scheme have two free parameters and its represented by the following family [23]:

$$\begin{aligned}\frac{1}{\Delta t}\left[a_1\mathbf{O}^{n+1}+a_2\mathbf{O}^{n}+a_3\mathbf{O}^{n-1}\right] &= b_1 f(\mathbf{O}^n)+b_2 f\left(\mathbf{O}^{n-1}\right)\\ &\quad + d\left[c_1 g\left(\mathbf{O}^{n+1}\right)+c_2 g(\mathbf{O}^n)\right]\\ &\quad + d\left[c_3 g\left(\mathbf{O}^{n-1}\right)\right]\end{aligned} \tag{5.1}$$

Where Δt is the time step, $a_1 = \gamma + 1/2$, $a_2 = -2\gamma$, $a_3 = \gamma - 1/2$, $b_1 = \gamma + 1$, $b_2 = -\gamma$, $c_1 = \gamma + \beta/2$, $c_2 = 1 - \gamma - \beta$, $c_3 = \beta/2$ and γ, β the free parameters. As it can be seen, a second-order IMEX scheme is a two-step method, i.e. one require two previously known values to compute the next one, and an initialization step is usually required.

Some selections of the free parameters lead to quite well known schemes, e.g. selecting $(\gamma, \beta) = (1/2, 0)$ leads to a second-order Adams-Bashforth formulation for the explicit part and a Crank-Nicolson for the implicit part and selecting $(\gamma, \beta) = (0, 1)$ leads to a leap frog formulation for the explicit part and a Crank-Nicolson for the implicit part.

For more details regarding second-order IMEX schemes and multi-step IMEX schemes in general see Ascher, Ruuth, and Wetton [23] and Ruuth [24].

5.1.5 Pressure Correction Method for Incompressible, Time Depend Flows

For time-dependent, incompressible flows a common way to solve the discretized equation is the projection or pressure correction method [16]. In general, it consists of a basic iterative procedure between the velocity and pressure fields [21]. Here in a prediction step, the velocity field is determined from the momentum equation. This velocity field does not satisfy the divergence free condition and needs to be corrected. The predicted velocity field is then employed in a projection or correction step, which leads to a Poisson equation for the pressure subject to a Neumann boundary condition. Finally, once the Poisson equation has been solved, the obtained pressure is used to correct the velocity field so it complies with the divergence free condition. It must be commented that the pressure correction method is a discrete version of the projection of a function on a divergence free space, see 1.8 of Henningson and Berggren [16] for details.

Also it must be noted, that the splitting (into prediction/correction steps) typically takes place after the time discretization has been done.

5.2 Discretized Form of Governing Equations

5.2.1 Summary of Governing Equations

Recall the governing equations in non-dimensional form:

$$\frac{\partial u_i}{\partial x_i} = 0 \tag{5.2}$$

$$\frac{\partial u_i}{\partial t} = -\frac{\partial \left(u_i u_j\right)}{\partial x_j} - \frac{\partial \tilde{p}}{\partial x_i} + Pr\frac{\partial^2 u_i}{\partial x_j \partial x_j} + S_i + RaPrT\delta_{i2} \tag{5.3}$$

$$\frac{\partial T}{\partial t} + \frac{1}{St}\frac{\partial f_l}{\partial t} = -\frac{\partial \left(T u_i\right)}{\partial x_i} + \frac{\partial^2 T}{\partial x_i \partial x_i} \tag{5.4}$$

Here all variables have been previously defined and to avoid cumbersome notation the $*$ super-index, in this chapter, has been dropped as a sign of a non-dimensional variable.

5.2.2 Spatial Discretization

A finite volume method is used for the spatial discretization. Due to the problem geometry (see figure 4.1) and to avoid spurious checkboard modes, a 2D Cartesian uniform staggered grid is to be employed. The control volume for the continuity and energy equations is centred around the pressure/temperature point while the control volume for the streamwise and normal velocities is centred around the streamwise and normal velocity points, respectively. See figure 5.1.

As previously mentioned, a finite volume formulation in a Cartesian uniform grid leads to second-order finite difference formulas. Hence:

$$\frac{u_{i+1/2,j} - u_{i-1/2,j}}{\Delta x} + \frac{v_{i,j+1/2} - v_{i,j-1/2}}{\Delta y} = 0 \tag{5.5}$$

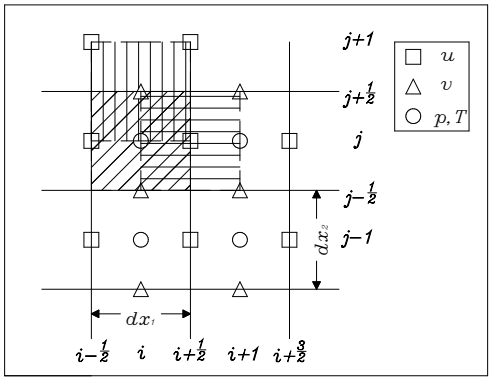

Figure 5.1: Staggered Cartesian grid employed for the finite volume formulation of the governing equations.

$$\begin{aligned}\frac{\partial u_{i+1/2,j}}{\partial t} = &-\frac{(uu)_{i+1,j}-(uu)_{i,j}}{\Delta x}-\frac{(uv)_{i+1/2,j+1/2}-(uv)_{i+1/2,j-1/2}}{\Delta y}\\ &-\frac{\tilde{p}_{i+1.j}-\tilde{p}_{i,j}}{\Delta x}+Pr\left[\frac{u_{i+3/2,j}-2u_{i+1/2,j}+u_{i-1/2,j}}{\Delta x^2}\right]\\ &+Pr\left[\frac{u_{i+1/2,j+1}-2u_{i+1/2,j}+u_{i+1/2,j-1}}{\Delta y^2}\right]+S_{i+1/2,j}\end{aligned} \tag{5.6}$$

$$\begin{aligned}\frac{\partial v_{i,j+1/2}}{\partial t} = &-\frac{(uv)_{i+1/2,j+1/2}-(uv)_{i-1/2,j+1/2}}{\Delta x}-\frac{(vv)_{i,j+1}-(vv)_{i,j}}{\Delta y}\\ &-\frac{\tilde{p}_{i.j+1}-\tilde{p}_{i,j}}{\Delta y}+Pr\left[\frac{v_{i+1,j+1/2}-2v_{i,j+1/2}+v_{i-1,j+1/2}}{\Delta x^2}\right]\\ &+Pr\left[\frac{v_{i,j+3/2}-2v_{i,j+1/2}+v_{i,j-1/2}}{\Delta y^2}\right]+S_{i,j+1/2}\\ &+RaPrT_{i,j+1/2}\end{aligned} \tag{5.7}$$

$$\begin{aligned}\frac{\partial T_{i,j}}{\partial t}+\frac{1}{St}\frac{\partial f_{l\,i,j}}{\partial t} = &-\frac{(uT)_{i+1/2,j}-(uT)_{i-1/2,j}}{\Delta x}\\ &-\frac{(vT)_{i,j+1/2}-(vT)_{i,j-1/2}}{\Delta y}\\ &+\frac{T_{i+1,j}-2T_{i,j}+T_{i-1,j}}{\Delta x^2}+\frac{T_{i,j+1}-2T_{i,j}+T_{i,j-1}}{\Delta y^2}\end{aligned} \tag{5.8}$$

Where: $u_{i+1,j} \approx 0.5\left(u_{i+3/2,j}+u_{i+1/2,j}\right)$, $u_{i,j} \approx 0.5\left(u_{i+1/2,j}+u_{i-1/2,j}\right)$, $u_{i+1/2,j+1/2} \approx 0.5\left(u_{i+1/2,j}+u_{i+1/2,j+1}\right)$, $v_{i+1/2,j+1/2} \approx 0.5\left(v_{i,j+1/2}+v_{i+1,j+1/2}\right)$, $u_{i+1/2,j-1/2} \approx 0.5\left(u_{i+1/2,j}+u_{i+1/2,j-1}\right)$, $v_{i+1/2,j-1/2} \approx 0.5\left(v_{i,j-1/2}+v_{i+1,j-1/2}\right)$, $u_{i-1/2,j+1/2} \approx 0.5\left(u_{i-1/2,j}+u_{i-1/2,j+1}\right)$, $v_{i-1/2,j+1/2} \approx 0.5\left(v_{i,j+1/2}+v_{i-1,j+1/2}\right)$, $v_{i,j+1} \approx 0.5\left(v_{i,j+1/2}+v_{i,j+3/2}\right)$, $v_{i,j} \approx 0.5\left(v_{i,j+1/2}+v_{i,j-1/2}\right)$, $T_{i,j+1/2} \approx 0.5\left(T_{i,j}+T_{i,j+1}\right)$, $T_{i+1/2,j} \approx 0.5\left(T_{i+1,j}+T_{i,j}\right)$, $T_{i-1/2,j} \approx 0.5\left(T_{i-1,j}+T_{i,j}\right)$, $T_{i,j-1/2} \approx 0.5\left(T_{i,j}+T_{i,j-1}\right)$, $f_{l\,i+1/2,j} \approx 0.5\left(f_{l\,i+1,j}+f_{l\,i,j}\right)$, and $f_{l\,i,j+1/2} \approx 0.5\left(f_{l\,i,j+1}+f_{l\,i,j}\right)$.

In the expressions above, the Darcy type source term is according to equation (3.10), see chapter 3, with phase change interval and morphology constant set to 1×10^{-3} and to 1.6×10^{6}, respectively. Such values are used by Binet and Lacroix in their algorithm according to Bertrand et al. [8].

The sub-indices represent discrete spatial positions of the domain with $n_x \times n_y$ cells for $i = 0, 1, \ldots, n_x, n_{x+1}$, $j = 0, 1, \ldots, n_y, n_{y+1}$ and spatial steps $\Delta x = (L/H)/n_x$, $\Delta y = (H/H)/n_y$. Thus, (5.5)-(5.8) is a system of discrete algebraic equations that is to be solved for the unknown quantities.

As defined in figure 5.1, on the staggered grid, the pressure and temperature discrete fields are defined in the cell midpoints whilst the streamwise and normal velocities are defined on the vertical and horizontal cell interfaces, respectively. Consequently, the interior resolution (not considering boundary points nor "ghost" points outside the domain) for the different quantities is: $n_x \times n_y$ for pressure, temperature, and liquid fraction fields, $(n_x - 1) \times n_y$ for the streamwise velocity, and $n_x \times (n_y - 1)$ for the normal velocity. Most computations are performed with an 80×80 grid size.

5.2.3 Boundary Conditions

As seen in figure 4.1(*a*), in the previous chapter, for the velocity field there are prescribed Dirichlet boundary conditions all around the 2D cavity whilst for the temperature field there are prescribed Dirichlet boundary conditions for the left and right wall and Neumann boundary conditions for the upper and lower wall.

To illustrate the numerical treatment of the boundary conditions consider the upper wall where $u\left(x, y=1\right) = v\left(x, y=1\right) = 0$ and $\partial T\left(x, y=1\right)/\partial y = 0$. Since the normal velocity component is defined on the vertical cell interfaces, the corresponding condition can be expressed directly as $v_{i,n_{y+1/2}} = 0$. This is not the case for the other two conditions.

The nonslip condition and the adiabatic boundary condition in this case are applied indirectly during the estimation of "ghost" point values. Such points are outside the domain and appear while expressing the discrete form of the governing equations, e.g. consider the term $u_{i+1/2,n_{y+1}}$ in the streamwise momentum equation and the term $T_{i,n_{y+1}}$ in the thermal energy equation at $j = n_y$. For the first example, through extrapolation one can find the "ghost" point value i.e. $u_{i+1/2,n_{y+1}} = 2u\left(x, y=1\right) - u_{i,n_y}$ which due to the non-slip boundary condition implies that $u_{i+1/2,n_{y+1}} = -u_{i,n_y}$. For the second example, $T_{i,n_{y+1}} = T_{i,n_y}$ due to the Neumann boundary condition.

An analogous numerical treatment is used for the others boundaries.

5.2.4 Temporal Discretization

The integration in time is done through a second order IMEX method treating all advective terms explicitly while all other terms are treated implicitly. The IMEX method employed is Adams-Bashforth/Modified Crank-Nicolson scheme were the free parameters (γ, β) are set to 0.5 and 1 respectively. The problem is initialized using a first order IMEX backward/forward Euler scheme (the advective terms are integrated using the explicit Euler method while all other terms are integrated using the implicit Euler method). A simple CFL condition is used to estimate the necessary time stepping for numerical stability; however most computations are performed with a non-dimensional time step of 2×10^{-5}. To enforce the divergence free condition, a projection-correction method is used and the iterative process to obtain the liquid

fraction is done through fixed point iteration as described in section 5.2.5.

In general, the time integration leads to equations similar to equation (5.1), see section 5.1.4. To exemplify the time integration procedure, consider the spatial discretized streamwise momentum equation which may be recast as:

$$\frac{d\mathbf{U}}{dt} = ADV_x(\mathbf{U}) + PrDIFF_x(\mathbf{U}) + DS_x(\mathbf{U}) - D_x(P) \tag{5.9}$$

Where: $\mathbf{U}$ is a vector representing the discrete streamwise velocity component, $ADV_x(\mathbf{U})$ represents the discrete, non-linear, advective term in equation (5.6), $DIFF_x(\mathbf{U})$ represents the discrete, linear, viscous diffusion term in equation (5.6), $DS_x(\mathbf{U})$ represents the Darcy type source term in equation (5.6), P is a vector representing the discrete pressure field, and $D_x(P)$ represents the discrete form of the pressure gradient in equation (5.6).

Equation (5.9) can then be integrated as:

$$\begin{aligned}\frac{a_1\mathbf{U}^{n+1}}{\Delta t} = &-\frac{1}{\Delta t}\left[a_2\mathbf{U}^n + a_3\mathbf{U}^{n-1}\right] \\ &+ b_1 ADV_x(\mathbf{U}^n) + b_2 ADV_x\left(\mathbf{U}^{n-1}\right) \\ &+ c_1\left[PrDIFF_x\left(\mathbf{U}^{n+1}\right) + DS_x\left(\mathbf{U}^{n+1}\right)\right] \\ &+ c_2\left[PrDIFF_x\left(\mathbf{U}^n\right) + DS_x\left(\mathbf{U}^n\right)\right] \\ &+ c_3\left[PrDIFF_x\left(\mathbf{U}^{n-1}\right) + DS_x\left(\mathbf{U}^{n-1}\right)\right] - D_x\left(P^{n+1}\right)\end{aligned} \tag{5.10}$$

At this point, the operations are split, i.e. to enforce the divergence free condition, a projection-correction method is used.

Prediction step:

$$\begin{aligned}\frac{a_1\mathbf{U}^*}{\Delta t} = &-\frac{1}{\Delta t}\left[a_2\mathbf{U}^n + a_3\mathbf{U}^{n-1}\right] \\ &+ b_1 ADV_x(\mathbf{U}^n) + b_2 ADV_x\left(\mathbf{U}^{n-1}\right) \\ &+ c_2\left[PrDIFF_x\left(\mathbf{U}^n\right) + DS_x\left(\mathbf{U}^n\right)\right] \\ &+ c_3\left[PrDIFF_x\left(\mathbf{U}^{n-1}\right) + DS_x\left(\mathbf{U}^{n-1}\right)\right]\end{aligned} \tag{5.11}$$

$$\frac{a_1}{\Delta t}\left[\mathbf{U}^{**} - \mathbf{U}^*\right] = c_1\left[PrDIFF_x\left(\mathbf{U}^{**}\right) + DS_x\left(\mathbf{U}^{**}\right)\right] \tag{5.12}$$

Correction step:

$$\frac{a_1}{\Delta t}\left[\mathbf{U}^{n+1} - \mathbf{U}^{**}\right] = -D_x\left({P_{num}}^{n+1}\right) \tag{5.13}$$

As it can be seen equation (5.11) is to be solved explicitly whilst equation (5.12) is to be solve implicitly. The corrected velocity is then recovered from equation (5.13) taking into account that P_{num} is given by the solution of the Poisson equation subject to a Neumann boundary condition as described in section 5.1.5 (i.e. the discrete form of P_{num} gradient vanish at the boundaries). The sub-index num is employed to clarify that the P_{num} quantity is not the actual pressure.

5.2.5 Iterative Process to Obtain Temperature and Liquid Fraction Fields

The iterative process to obtain the temperature and liquid fraction fields is done in the following manner: (1) the non-dimensional temperature is calculated using the liquid fraction corresponding to previous iteration, (2) the non-dimensional enthalpy is calculated using the non-dimensional temperature corresponding to the current iteration, (3) the liquid fraction is updated using the non-dimensional form of equation (3.6), (4) the error is calculated according to equation (5.14), (5) if the error is below the set tolerance the iteration has finished otherwise go back to (1). The tolerance tol used for all calculation was 1×10^{-8}. Initially the liquid fraction is set to the value corresponding to the previous time step.

$$\left| \frac{\max_{i,j} \left({\phi_{i,j}}^{n+1} - {\overline{\phi}_{i,j}}^{n+1} \right)}{\max_{i,j} \left({\overline{\phi}_{i,j}}^{n+1} \right) - \min_{i,j} \left({\overline{\phi}_{i,j}}^{n+1} \right)} \right| \leq tol \tag{5.14}$$

In equation (5.14), ${\phi_{i,j}}^{n+1}$ is the matrix representing the values of the newly calculated field (temperature or liquid fraction) and ${\overline{\phi}_{i,j}}^{n+1}$ the field from the previous iteration step.

5.2.6 General Solution Procedure

The solution procedure may be summarized as follows: (1) initialization, (2) beginning of time step, (3) new temperature and liquid fraction fields are obtained through iterative procedure, (4) velocity field is predicted not fulfilling continuity, (5) Poisson's equation is solved to enforce divergence free condition, (6) new velocity field, now corrected, is obtained, (7) go back to (2). It must be commented that the initialization procedure comprise steps (2) to (6).

Chapter 6

Results and Discussions

Figures 6.1-6.3 present the results corresponding to case 1 and 2 whilst figure 6.4 the results corresponding to the rest of the cases. The local melting front position is defined as the location where the local liquid fraction is equal to 0.99. The average melting front location ${s^*}_{av}$ and the average Nusselt number Nu_{av} are computed as in Jany and Bejan [12]:

$$ {s^*}_{av}\left(t^*\right) = \int_0^1 s^*\left(y^*, t^*\right)\ dy^* \tag{6.1} $$

$$ Nu_{av}\left(t^*\right) = -\int_0^1 \frac{\partial T^*}{\partial x^*}\left(x^* = 0, y^*, t^*\right)\ dy^* \tag{6.2} $$

In the expressions above the $*$ super-index signifies a non-dimensional variable.

The results obtained from the runs corresponding to test case 1 and 2 appear to be in good agreement with the main trend of results shown in benchmark Bertrand et al. [8] and Gobin and Le Quéré [9] and with Huber et al. [10]. Figure 6.2(*a*) also shows a grid resolution test. It is worth noted the oscillatory behaviour of the results obtained for test case 2 in figure 6.2(*b*). This behaviour is reported by Le Quéré and Couturier-Sadat in Bertrand et al. [8] and it was first observed by Dantzig [25], confirmed by a stability study in Le Quéré and Gobin [26], and reported by Gobin and Le Quéré [9]. According to the conclusions in Le Quéré and Gobin [26], it appears that the natural convection flow resulting from melting of a pure substance with a low Prandtl number, which it is heated from the side, it is prone to the classical multicellular instability for sufficiently large Rayleigh numbers. As it can be seen in figure 6.3, as the melting advances, the small

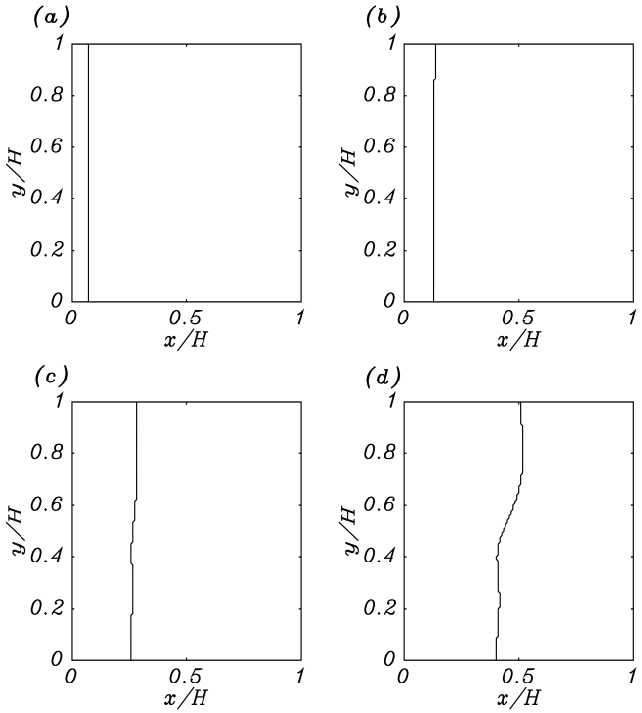

Figure 6.1: Melting front profile corresponding to test case 1: (*a*) $StFo = 0.004$, (*b*) $StFo = 0.01$, (*c*) $StFo = 0.04$, (*d*) $StFo = 0.1$. Here $Fo = (\alpha t)/H^2$ represents the Fourier number.

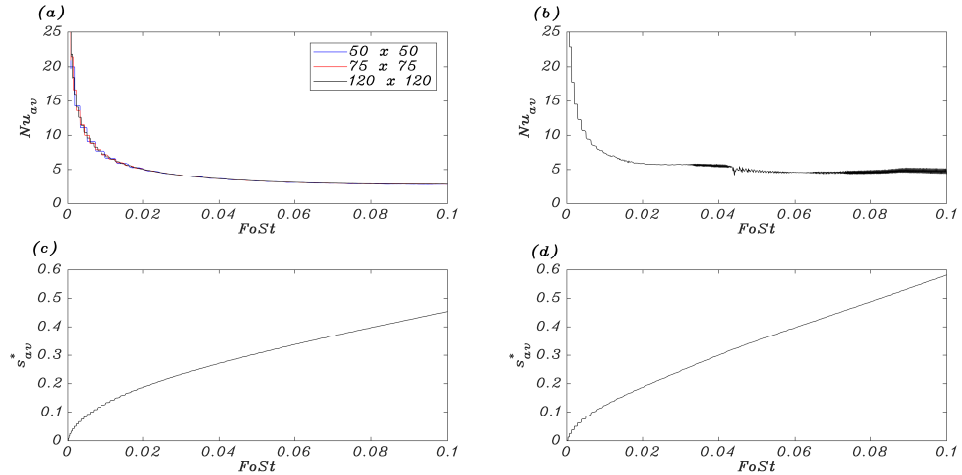

Figure 6.2: Average Nusselt number at the hot wall and average melting front position for test case 1 and 2: (*a*) Nu_{av} for test case 1, (*b*) Nu_{av} for test case 2, (*c*) $s^*{}_{av}$ for test case 1, (*d*) $s^*{}_{av}$ for test case 2.

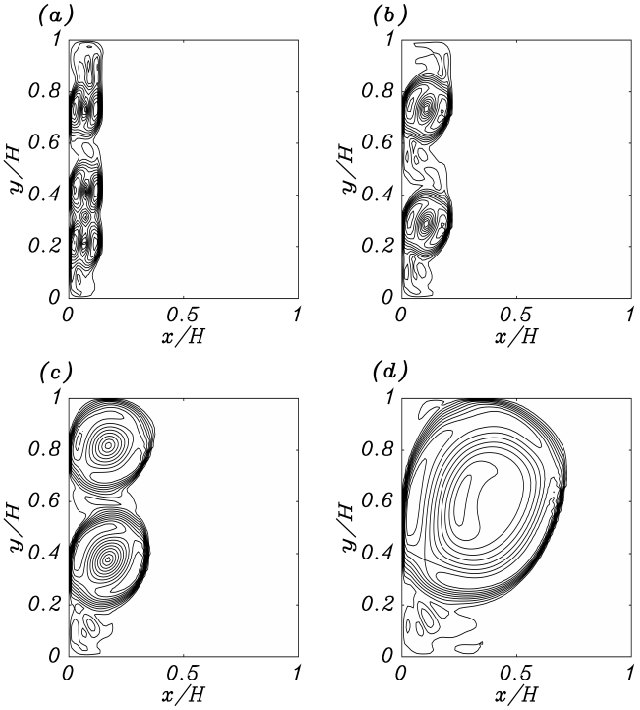

Figure 6.3: Flow structure corresponding to test case 2: (*a*) $StFo = 0.01$, (*b*) $StFo = 0.02$, (*c*) $StFo = 0.04$, (*d*) $StFo = 0.1$.

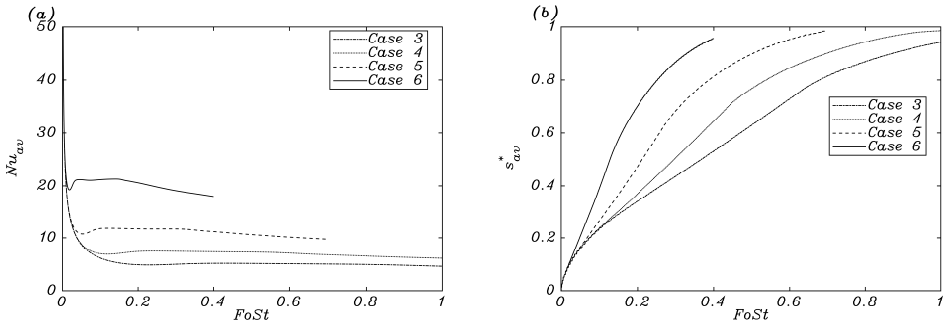

Figure 6.4: Average Nusselt number at the hot wall and average melting front position for test cases 3-6: (*a*) Nu_{av}, (*b*) $s^*{}_{av}$.

cells merge causing the high frequency oscillations observed in figure 6.2(*b*). This instability strongly affects the Nusselt number and the melting front position.

Regarding test cases 3-6, the obtained results appear to qualitatively agree with those reported in Huber et al. [10] until the liquid-solid interface reaches the right wall. After this event, the time evolution of the average Nusselt number differ due to the difference in the boundary condition. It is also interesting to note that the time evolution trend is similar to those of Jany and Bejan [12]. Huber et al. [10] reported more time variability in the results for a high value of Ra and attributed the behaviour to the low Prandlt number employed ($Pr = 1$). However, such difference might be due to the numerical scheme and not due to Pr.

For a quantitative comparison the correlations reported in Jany and Bejan [12] and Gobin and Bénard [11] and Huber et al. [10] are to be considered. Jany and Bejan [12] identified the basic regimes (view figure 3.2) and scales during the melting of a pure substance, driven by natural convection in the melt, inside a rectangular cavity. Jany and Bejan [12] at the end of the paper, also recognized and outline three possible extensions to their scaling theory: the effect of thermal inertia (i.e. the Stefan number), the low Prandtl number limit, and the effect of transient conduction in the solid phase. The first effect is studied in Huber et al. [10] while the second is studied in Gobin and Bénard [11]. The last effect must be taken into account when the initial temperature of the solid does not coincide with the melting temperature.

Table 6.1 summarized the correlations obtained by Jany and Bejan [12] and Gobin and Bénard [11] and Huber et al. [10] corresponding to the low and high Stefan number ranges.

Gobin and Bénard [11] noted in their results that the time evolution of the average Nusselt number in the transition regime depends on the dimensionless group $RaPr$ instead of Ra, as suggested by Jany and Bejan [12], and hence there is a different scaling for the low Pr number range. From the data obtained, for case 1 and 2, the ratio $Nu_{end}/\left(Ra^{0.27}Pr^{0.18}\right)$ is equal to 0.37 and to 0.36, respectively. Such values agree with the scaling proposed by Gobin and Bénard [11]. Here the sub-index end indicate the last average Nusselt number in the dataset corresponding to the computation. It must be noted that the scaling law reported by Gobin and Bénard [11], is obtained assuming quasi-steady conditions and in case 2 such conditions do not

Table 6.1: Correlations corresponding to the end of the mixed regime (identified by the sub-index min) and the end of the convective regime (identified by the sub-index 2). In the case of $Pr < O(1)$ is assumed that there is no contact with the cold wall and Nu_2 represents a quasi-steady average Nusselt number in the convective regime. Low and high St denote the low and high range of the Stefan number, respectively.

		Nu_{min}	$FoSt_{min}$	Nu_2	$FoSt_2$
Low St	$Pr < O(1)$	$\sim$	$\sim$	$0.29Ra^{0.27}Pr^{0.18}$	$\sim$
	$Pr > O(1)$	$0.28Ra^{1/4}$	$9Ra^{-1/2}$	$0.35Ra^{1/4}$	$1.8Ra^{-1/4}$
High St	$Pr > O(1)$	$0.31Ra^{1/4}$	$56Ra^{-1/2}$	$0.29Ra^{1/4}$	$8.7Ra^{-1/4}$

happen. Consequently, for case 2, it might be more appropriate to calculate the simple or quadratic mean of the last dataset group to estimate Nu_2. Also, for case 1, it is likely that Nu_{end} does not correspond to Nu_2 and the code needs to be run for a higher value of $FoSt$ (in Gobin and Bénard [11] the time evolution of the average Nusselt number is consider up to $FoSt = 0.25$ and here up to 0.1). In such instance it might be more appropriate to compare Nu_{end} to the corresponding average Nusselt number calculated through the canonical expression recommended by Churchill [27] with the three constants suggested by Gobin and Bénard [11].

Figure 6.5 presents the scaling corresponding to the data obtained from the computations of cases 3-6.

As it can been seen from figure 6.5, the obtained results are in good agreement with the scaling laws and the correlations reported by Huber et al. [10]. However, in contrast with Huber et al. [10], for all computation the obtained average Nusselt number corresponding to the end of the convection regime is slightly higher than the minimum value corresponding to the end of the mixed regime. This behaviour is also observed in the results of Jany and Bejan [12].

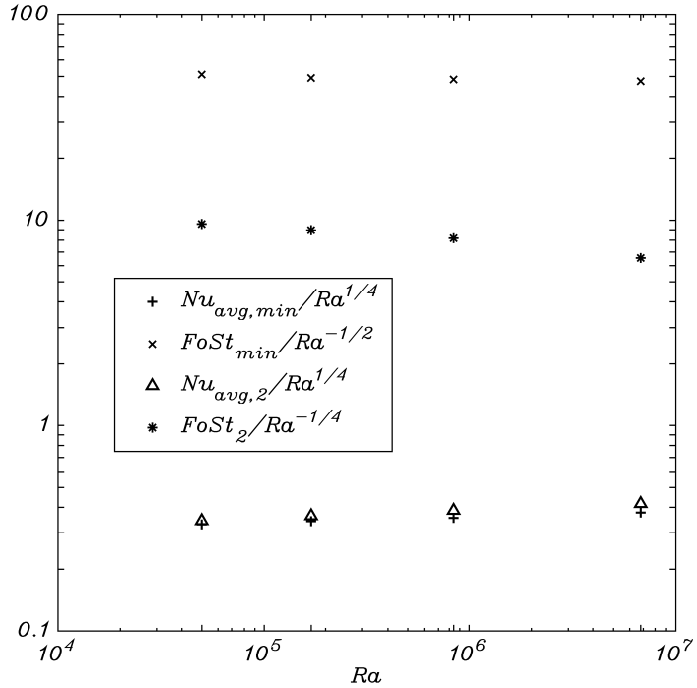

Figure 6.5: Scaling from the numerical modelling corresponding to the high Stefan number range.

Chapter 7

Conclusions and Further Work

A classic finite volume method is used to numerically handle the fusion of a pure substance.

Results obtained in the present study, show good agreement with the main trend of the compared literature. The Rayleigh number is shown to be the key parameter in natural convection. For given Prandtl and Stefan numbers, as Ra increases, the deviation from conduction dominating regime occurs at earlier times and both melting rate and heat transfer increase. See the temporal evolution of average liquid fraction and average Nusselt number in figures 6.2 and 6.4.

However, in contrast with the results of Huber et al. [10], some differences are observed. For all computation, the average Nusselt number corresponding to the contact of the liquid-solid interface with the right wall (at the end of the convection regime) is slightly higher than the minimum value. Also, the curves present a similar time variability to the one reported by Jany and Bejan [12] even for a high value of Ra.

There might be other quantitative differences as well. As noticed in Bertrand et al. [8] and Gobin and Le Quéré [9] where multiple methods are compared, this is probably due to differences in the order of accuracy of the space or time discretization scheme or grid refinement. Or even due to the scheme itself, e.g. an upwind scheme treatment of the advective terms might lead to an underestimation of the average Nusselt number for high Ra or to the introduction of artificial diffusion.

Nonetheless it is concluded that Ra is fundamental for the onset of natural convection and that the thermal inertia and the low Prandtl number range have an effect over the melting problem and the heat transfer correlations developed by Jany and Bejan [12].

It is worth noted that the model employed here could be modified, possible with relatively ease, to do new research in the field.
As previously commented, due to PCMs capacity as thermal energy stores, the study of phase change problems has grown during the last years. In the previous chapters, a relatively simple case where melting is driven by natural convection in the melt is studied. The idea was to develop a working algorithm that could be modified with relative ease in further work.

Motivated by the present study and recent publications, the following topics may be proposed:
(1) Study of phase change problems where a PCM inside a rectangular cavity is subject to different thermal boundary conditions. Typically the rectangular cavity is subject to constant temperature (in applications such as melting of pure metals) or constant heat flux boundary conditions (in applications such as waste heat recovery, solar energy, or cooling systems). However one could decide to study discrete or continuum spatial depending thermal boundary condition. Example of such studies includes Lakhal et al. [28] and Sarris, Lekakis, and Vlachos [29]. Equally one could decide to include radiative boundary conditions.
(2) Study of phase change problems where a PCM inside a rectangular cavity is subject to different effects. In Yao et al. [30] volumetric radiation is included in the analysis of the melting problem, which it is of particular interest since all heat transfer mechanism are included in the study. In Madruga and Mendoza [31] thermocapillary effects are taken into account through the boundary conditions. In Doostanidezfuli, Ghalambaz, and Chamkha [32] and Colaço, Dulikravich, and Martin [33] the effects of a magnetic field and an electric field are taken into account, respectively. In Zennouhi et al. [34] the effect of the cavity inclination angle is considered and in Kozak and Ziskind [35] solid bulk motion is treated. In Qarnia, Draoui, and Lakhal [36] protruding heat sources are added to the PCM.
Possible studies could combine some of such effects, for example in Pirmohammadi and Ghassemi [37] the effect of a magnetic field and the inclination of the cavity are considered. And more recently in Joneidi et al. [38] the effect of heat flux and inclination angle variation in a rectangular PCM containing cavity was experimentally investigated.
Studies concerning the inclination angle could be particular interest-

ing since it can effectively affect the time evolution and trend of the heat transfer in the melting problem in an almost cost free manner for storage system applications based on PCMs.
(3) Another possibility could be to study phase change problems where a PCM inside a rectangular cavity is subject to different effects and other boundary conditions. An example is El Khaoudi et al. [39] where the cavity is linearly heated from the side and the effect of a magnetic field is taken into account.
(4) Study phase change problems taking into account the possibility of non-constant thermosphysical properties both in the liquid and in the solid due to high temperature differences in the initial and/or boundary conditions. As an example consider Rihab et al. [40] where a study of heat conduction during melting of PCMs with different thermophysical properties is performed.
(5) Study of phase change problems where the PCMs is not a pure substance and the mushy zone region is not a numerical artefact. In this case, the advection of the liquid fraction needs to be accounted for in the energy equation.
(6) A numerical study concerning a rectangular PCM containing cavity taking into account volumetric expansion/contraction due to melting/solidification through an elastic wall. Dallaire and Gosselin [41] for example, studied the solidification of water, as PCM, inside the cavity taking into account the density change during the phase change and resulting in the deformation of the wall cavity due to the expansion. This study was implemented through Fluent, Ansys 17.0 commercial software.
(7) Scaling laws for phase change problems where the effect of transient conduction in the solid phase is taken into account. This is one of the possible extensions for the scaling theory published by Jany and Bejan [12] and it is of interest since even in laboratory experiment is difficult to maintain the solid uniformly at the melting temperature.
(8) Study of the flow structure in the melting of the PCM inside the rectangular cavity driven by natural convection in the melt for the low Prandtl number range and relatively high Rayleigh numbers. As observed by Dantzig [25] and studied by Le Quéré and Gobin [26] for this case, an apparent instability in the flow takes place at the end of the conduction regime. This instability later leads to a secondary oscillatory instability (view figure 6.2(*b*)) which strongly affects the heat transfer and the melting front position, as reported in Bertrand et al.

[8] and Gobin and Le Quéré [9]. In Le Quéré and Gobin [26] the authors recognized as limitations in their analysis the assumptions of a quasi-steady base flow and that the instability develops rapidly compared to the slow time scale evolution. It is also worth noted that they performed a linear stability analysis.
(9) Suitability, from a numerical stability point of view, of certain methods to solve phase change problems. An example of this type of study for time dependent diffusion-advection problems is done by Ascher, Ruuth, and Wetton [23]. Second order IMEX schemes are particularly convenient since the employed algorithm used such method.
(10) Numerical studies of heat transfer enhancement techniques in PCMs. Most PCMs have unacceptably low thermal conductivity, leading to slow charging/discharging rates [1] and required a way to enhance the heat transfer. Agyenim et al. [1] reported that due to simplicity, ease in fabrication, and low cost during construction, the majority of heat enhancement are based on the application of fin embedded in the PCM followed by the used of metal matrix, where the metal presents high conductivity, into the PCM. A possible set up could be the use of fins of determined aspect ratio inside a rectangular cavity with the purpose of study the flow structure and the heat transfer enhancement with respect to a configuration without the fins.

Appendix A

Additional Validation: Conductive Melting

As additional validation, pure conductive melting inside the 2D cavity is considered. As with the convective melting, the boundary and initial conditions are depicted in figure 4.1(*a*).
The computations are performed with a 100×5 grid size and a non-dimensional time step of 2×10^{-4}.

Figure A.1, for three different Stefan numbers, shows the dimensionless melting front position as a function of the Fourier number and the dimensionless temperature profile as a function of the normalized x-coordinate.
Results are compared with the corresponding analytic solutions in the liquid half-space i.e. Neumann solution in the liquid region for the Stefan problem, see equations (A.1)-(A.3). As it can be seen, the numerical and analytical results are in good agreement.

$$\zeta \exp\left(\zeta^2\right) \operatorname{erf}\left(\zeta\right) = \frac{St}{\sqrt{\pi}} \tag{A.1}$$

$$s^*\left(Fo\right) = 2\zeta\sqrt{Fo} \tag{A.2}$$

$$T^*\left(x^*, Fo\right) = 1 - \frac{\operatorname{erf}\left[x^* / \left(2\sqrt{Fo}\right)\right]}{\operatorname{erf}\left(\zeta\right)}, \quad 0 \leq x^* \leq s^*\left(Fo\right) \tag{A.3}$$

In the expressions above ζ is a coefficient implicitly dependent of the Stefan number, exp is the exponential function and erf is the error function.

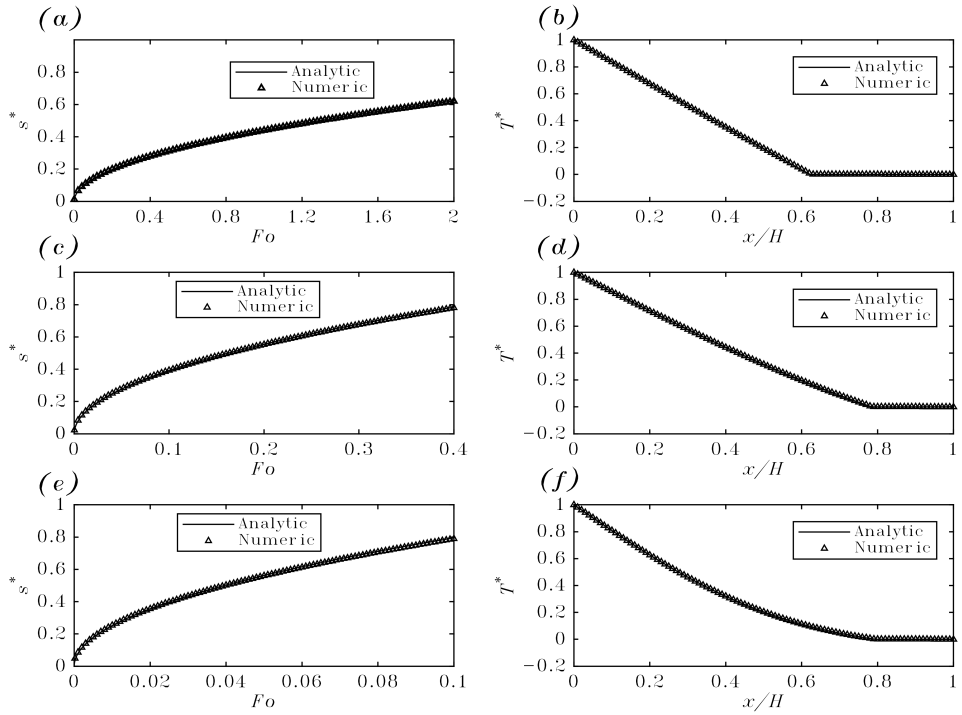

Figure A.1: Comparison of dimensionless melting front position and dimensionless temperature profile for pure conductive melting: (*a*) s^* as a function of Fo for $St = 0.1$, (*b*) T^* as a function of x/H for $FoSt = 0.2$, (*c*) s^* as a function of Fo for $St = 1$, (*d*) T^* as a function of x/H for $FoSt = 0.4$, (*e*) s^* as a function of Fo for $St = 10$, (*f*) T^* as a function of x/H for $FoSt = 1$.

Appendix B

MATLAB Code and Numerical Data

The developed code is available through: `https://www.dropbox.com/sh/u9rrb17bwo29x2f/AAB3SYil3S9N4wzdI4iYhFKoa?dl=0`.
Also you could email to: `a.a.arosemena@gmail.com` to request the code.

To run it in `MATLAB R2016a` or in a more recent version, uncompress and place all files in a `MATLAB` local folder, open the `Ns_conv.m script` and press run.

For the current setting, the code solves case 1 (see section 4.2) in an 80×80 grid. At the end of the computation, the code creates a `.mat` file for post-processing in the local folder and gives the user the option of visualizing the solution (e.g. divergence, velocity field and temperature field, time evolution of the average Nusselt number and liquid fraction, or melting fronts). See figure B.1.

The numerical data for post-processing corresponding to case 1 in a 120×120 grid can also be access through the `Test_case_1.mat` file without executing the code.

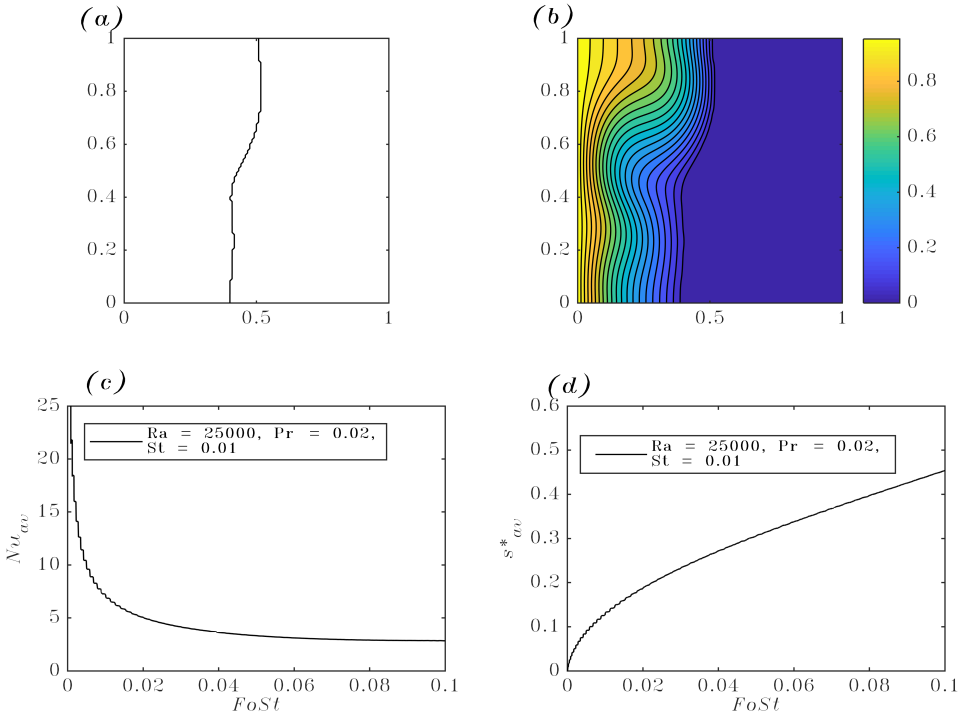

Figure B.1: Example of obtained data from code after case 1 computation: (*a*) melting front, (*b*) temperature field, (*c*) average Nusselt number, (*d*) average melting front position.

Bibliography

[1] F. Agyenim et al. “A review of materials, heat transfer and phase change problem formulation for latent heat thermal energy storage systems (LHTESS)”. In: *Renewable and Sustainable Energy Reviews* 14.2 (2010), pp. 615–628.

[2] B. Zalba et al. “Review on thermal energy storage with phase change: materials, heat transfer analysis and applications”. In: *Applied Thermal Engineering* 23.3 (2003), pp. 251–283.

[3] M. M. Farid et al. “A review on phase change energy storage: materials and applications”. In: *Energy Conversion and Management* 45.9 (2004), pp. 1597–1615.

[4] A. Sharma et al. “Review on thermal energy storage with phase change materials and applications”. In: *Renewable and Sustainable Energy Reviews* 13.2 (2009), pp. 318–345.

[5] R. Kandasamy, X.- Q. Wang, and A. S. Mujumdar. “Transient cooling of electronics using phase change material (PCM)-based heat sinks”. In: *Applied Thermal Engineering* 28.8 (2008), pp. 1047–1057.

[6] E.-B. S. Mettawee and G. M.R. Assassa. “Experimental study of a compact PCM solar collector”. In: *Energy* 31.14 (2006), pp. 2958–2968.

[7] F. Kuznik, J. Virgone, and J. Noel. “Optimization of a phase change material wallboard for building use”. In: *Applied Thermal Engineering* 28.11 (2008), pp. 1291–1298.

[8] O. Bertrand et al. “Melting driven by natural convection A comparison exercise: first results”. In: *International Journal of Thermal Sciences* 38.1 (1999), pp. 5–26.

[9] D. Gobin and P. Le Quéré. "Melting from an isothermal vertical wall. Synthesis of a numerical comparison exercise". In: *Computer Assisted Mechanics and Engineering Sciences* 7.3 (2000), pp. 289–306.

[10] C. Huber et al. "Lattice Boltzmann model for melting with natural convection". In: *International Journal of Heat and Fluid Flow* 29.5 (2008), pp. 1469–1480.

[11] D. Gobin and C. Bénard. "Melting of metals driven by natural convection in the melt: influence of Prandtl and Rayleigh numbers". In: *Journal of Heat Transfer* 114.2 (1992), pp. 521–524.

[12] P. Jany and A. Bejan. "Scaling theory of melting with natural convection in an enclosure". In: *International Journal of Heat and Mass Transfer* 31.6 (1988), pp. 1221–1235.

[13] R. B. Bird, W. E. Stewart, and E. N. Lightfoot. "The Subject of Transport Phenomena". In: *Transport Phenomena*. John Wiley and Sons, Inc., 2002, pp. 1–7.

[14] R. Aris. "The Kinematics of Fluid Motion". In: *Vectors, Tensors, and the Basic Equations of Fluid Mechanics*. Dover Publications, Inc., 1989, pp. 76–98.

[15] P. K. Kundu, I. M. Cohen, and D. R. Dowling. In: *Fluid Mechanics*. Academic Press, 2012.

[16] D. S. Henningson and M. Berggren. In: *Fluid Dynamics: Theory and Computation*. KTH Royal Institute of Technology, 2005.

[17] Y. A. Çengel and A. J. Ghajar. In: *Heat and Mass Transfer-Fundamentals and Applications*. McGraw-Hill Education, 2015.

[18] W. Shyy et al. "Fixed grid techniques: enthalpy formulation". In: *Computational Fluid Dynamics with Moving Boundaries*. Dover Publications, Inc, 2007, pp. 135–166.

[19] V.R. Voller and C. Prakash. "A fixed grid numerical modelling methodology for convection-diffusion mushy region phase-change problems". In: *International Journal of Heat and Mass Transfer* 30.8 (1987), pp. 1709–1719.

[20] A. D. Brent, V. R. Voller, and K. J. Reid. "Enthalpy-Porosity technique for modeling convection-diffusion phase change: application to the melting of a pure metal". In: *Numerical Heat Transfer* 13.3 (1988), pp. 297–318.

[21] C. Hirsch. In: *Numerical Computation of Internal and External Flows. Volume 1-Fundamentals of Computational Fluid Dynamics*. Butterworth-Heinemann, 2007.

[22] M. Schäfer. "Finite-Volume Methods". In: *Computational Engineering-Introduction to Numerical Methods*. Springer, 2006, pp. 77–105.

[23] U. M. Ascher, S. J. Ruuth, and B. T. R. Wetton. "Implicit-Explicit methods for time-dependent partial differential equations". In: *SIAM Journal on Numerical Analysis* 32.3 (1995), pp. 797–823.

[24] S. J. Ruuth. "Implicit-Explicit Methods for Time Dependent PDEs". Master Thesis. Vancouver, Canada: University of British Columbia, 1993.

[25] J. A. Dantzig. "Modelling liquid–solid phase changes with melt convection". In: *International Journal for Numerical Methods in Engineering* 28.8 (1989), pp. 1769–1785.

[26] P. Le Quéré and D. Gobin. "A note on possible flow instabilities in melting from the side". In: *International Journal of Thermal Sciences* 38.7 (1999), pp. 595–600.

[27] S. W. Churchill. "The development of theoretically based correlations for heat and mass transfer". In: *Latin American Journal of Heat and Mass Transfer* 7 (1983), pp. 207–229.

[28] E. Lakhal et al. "Natural convection in a square enclosure heated periodically from part of the bottom wall". In: *Numerical Heat Transfer, Part A: Applications* (1995), pp. 319–333.

[29] I. E. Sarris, I. Lekakis, and N. S. Vlachos. "Natural convection in a 2D enclosure with sinusoidal upper wall temperature". In: *Numerical Heat Transfer, Part A: Applications* 42.5 (2002), pp. 513–530.

[30] F.-J. Yao et al. "Analysis of melting with natural convection and volumetric radiation using lattice Boltzmann method". In: *International Journal of Heat and Mass Transfer* 112 (2017), pp. 413–426.

[31] S. Madruga and C. Mendoza. "Heat transfer performance and melting dynamic of a phase change material subjected to thermocapillary effects". In: *International Journal of Heat and Mass Transfer* 109 (2017), pp. 501–510.

[32] A. Doostanidezfuli, M. Ghalambaz, and A. Chamkha. "MHD natural convection phase-change heat transfer in a cavity: analysis of the magnetic field effect". In: *Journal of the Brazilian Society of Mechanical Sciences and Engineering* 39 (Feb. 2017), pp. 2831–2846.

[33] M. J. Colaço, G. S. Dulikravich, and T. J. Martin. "Optimization of wall electrodes for electro-hydrodynamic control of natural convection during solidification". In: *Materials and Manufacturing Processes* 19.4 (2004), pp. 719–736.

[34] H. Zennouhi et al. "Effect of inclination angle on the melting process of phase change material". In: *Case Studies in Thermal Engineering* 9 (2017), pp. 47–54.

[35] Y. Kozak and G. Ziskind. "Melting in a Rectangular Cavity". In: *ASME. Heat Transfer Summer Conference* 1 (2016).

[36] H. E. Qarnia, A. Draoui, and E. K. Lakhal. "Computation of melting with natural convection inside a rectangular enclosure heated by discrete protruding heat sources". In: *Applied Mathematical Modelling* 37.6 (2013), pp. 3968–3981.

[37] M. Pirmohammadi and M. Ghassemi. "Effect of magnetic field on convection heat transfer inside a tilted square enclosure". In: *International Communications in Heat and Mass Transfer* 36 (Aug. 2009), pp. 776–780.

[38] M. H. Joneidi et al. "Experimental investigation of phase change in a cavity for varying heat flux and inclination angles". In: *Experimental Thermal and Fluid Science* 88 (2017), pp. 594–607.

[39] F. El Khaoudi et al. "Numerical and theoretical modeling of natural convection of nanofluids in a vertical rectangular cavity. Investigate the effects of a magnetic field". In: *International Review of Mechanical Engineering (IREME)* 8.6 (2014), pp. 1102–1109.

[40] H. Rihab et al. "Enthalpic lattice Boltzmann formulation for heat conduction during melting of PCMs with embedded solid blocks with different thermophysical properties". In: *International Journal of Heat and Technology* 35 (June 2017), pp. 330–338.

[41] J. Dallaire and L. Gosselin. "Numerical modeling of solid-liquid phase change in a closed 2D cavity with density change, elastic wall and natural convection". In: *International Journal of Heat and Mass Transfer* 114 (2017), pp. 903–914.

[42] A. Faghri and Y. Zhang. "Melting and solidification". In: *Transport Phenomena in Multiphase Systems*. Academic Press, Elsevier Science, 2006, pp. 421–530.

[43] V. R. Voller and C. R. Swaminathan. "General Source-Based method for solidification phase change". In: *Numerical Heat Transfer, Part B: Fundamentals* 19.2 (1991), pp. 175–189.

[44] V. R. Voller, M. Cross, and N. C. Markatos. "An enthalpy method for convection/diffusion phase change". In: *International Journal for Numerical Methods in Engineering* 24.1 (1987), pp. 271–284.

[45] M. N. Özişik. In: *Heat Transfer-A Basic Approach*. McGraw-Hill Book Company, 1985.

[46] R. H. Pletcher, J. C. Tannehill, and D. A. Anderson. In: *Computational Fluid Mechanics and Heat Transfer*. CRC Press, 2013.